Observation and studies of jet quenching in PbPb collisions at √sNN=2.76 TeV

Journal Article

Author(s):

CMS Collaboration; Chatrchyan, Serguei; Bortignon, Pierluigi; Caminada, Lea; Chen, Zhiling; Cittolin, Sergio; Dissertori, Günther; Dittmar, Michael; Eugster, Jürg; Freudenreich, Klaus; Grab, Christoph; Hervé, Alain; Hintz, Wieland; Lecomte, Pierre; Lustermann, Werner; Marchica, Carmelo; Martinez Ruiz del Arbol, Pablo; Meridiani, Paolo; Milenovic, Predrag; Moortgat, Filip; Nef, Pascal; Nessi-Tedaldi, Francesca; Pape, Luc; Pauss, Felicitas; Punz, Thomas; Rizzi, Andrea; Ronga, Frédéric J.; Rossini, Marco; Sala, Leonardo; Sanchez, Ann-Karin; Sawley, Marie-Christine; Stieger, Benjamin; Tauscher, Ludwig; Thea, Alessandro; Theofilatos, Konstantinos; Treille, Daniel; Urscheler, Christina; Wallny, Rainer; Wehrli, Lukas; Weng, Joanna; et al.

Observation and studies of jet quenching in PbPb collisions at $\sqrt{s_{NN}} = 2.76$ TeV

S. Chatrchyan *et al.*[*]

(CMS Collaboration)

(Received 10 February 2011; published 12 August 2011)

Jet production in PbPb collisions at a nucleon-nucleon center-of-mass energy of 2.76 TeV was studied with the Compact Muon Solenoid (CMS) detector at the LHC, using a data sample corresponding to an integrated luminosity of 6.7 μb^{-1}. Jets are reconstructed using the energy deposited in the CMS calorimeters and studied as a function of collision centrality. With increasing collision centrality, a striking imbalance in dijet transverse momentum is observed, consistent with jet quenching. The observed effect extends from the lower cutoff used in this study (jet $p_T = 120$ GeV/c) up to the statistical limit of the available data sample (jet $p_T \approx 210$ GeV/c). Correlations of charged particle tracks with jets indicate that the momentum imbalance is accompanied by a softening of the fragmentation pattern of the second most energetic, away-side jet. The dijet momentum balance is recovered when integrating low transverse momentum particles distributed over a wide angular range relative to the direction of the away-side jet.

I. INTRODUCTION

High-energy collisions of heavy ions allow the fundamental theory of the strong interaction—quantum chromodynamics (QCD)—to be studied under extreme temperature and density conditions. A new form of matter [1–4] formed at energy densities above ~1 GeV/fm^3 is predicted in lattice QCD calculations [5]. This quark-gluon plasma (QGP) consists of an extended volume of deconfined and chirally symmetric quarks and gluons.

Heavy ion collisions at the Large Hadron Collider (LHC) are expected to produce matter at energy densities exceeding any previously explored in experiments conducted at particle accelerators. One of the first experimental signatures suggested for QGP studies was the suppression of high-transverse-momentum (p_T) hadron yields resulting from energy loss suffered by hard-scattered partons passing through the medium [6]. This parton energy loss is often referred to as "jet quenching." The energy lost by a parton provides fundamental information on the thermodynamical and transport properties of the traversed medium, which is now believed to be strongly coupled as opposed to an ideal gas of quarks and gluons (for recent reviews, see Refs. [7,8]). Results from nucleus-nucleus collisions at the Relativistic Heavy Ion Collider (RHIC) [9–12] have shown evidence for the quenching effect through the suppression of inclusive high-p_T hadron production and the modification of high-p_T dihadron angular correlations when compared to the corresponding results in much smaller systems, especially proton-proton collisions. Preliminary results for fully reconstructed jets at RHIC, measured in AuAu

collisions at $\sqrt{s_{NN}} = 200$ GeV [13–16], also hint at broadened jet shapes due to medium-induced gluon radiation.

Studying the modification of jets has long been proposed as a particularly useful tool for probing the QGP properties [17,18]. Of particular interest are the dominant "dijets," consisting of the most energetic ("leading") and second most energetic ("subleading") jets. At leading order (LO) and in the absence of parton energy loss, the two jets have equal p_T with respect to the beam axis and are emitted very close to back to back in azimuth ($\Delta\varphi_{\text{dijet}} = |\varphi_{\text{jet1}} - \varphi_{\text{jet2}}| \approx \pi$). However, medium-induced gluon emission can significantly alter the energy balance between the back-to-back jets and may give rise to large deviations from $\Delta\varphi_{\text{dijet}} \approx \pi$ [7,19–27]. Such medium effects in nuclear interactions are expected to be much larger than those due to higher-order gluon radiation, which is also present for jet events in proton-proton (pp) collisions. The study of medium-induced modifications of dijet properties can therefore shed light on the transport properties of the QCD medium formed in heavy-ion collisions.

The dijet analysis presented in this paper was performed using the data collected in 2010 from PbPb collisions at a nucleon-nucleon center-of-mass energy of $\sqrt{s_{NN}} = 2.76$ TeV at the Compact Muon Solenoid (CMS) detector. The CMS detector has a solid angle acceptance of nearly 4π and is designed to measure jets and energy flow, an ideal feature for studying heavy-ion collisions. A total integrated (PbPb) luminosity of 8.7 μb^{-1} was collected, of which 6.7 μb^{-1} has been included in this analysis. Recently, related results on a smaller data sample (1.7 μb^{-1}) have been reported by ATLAS [28].

Jets were reconstructed based on their energy deposits in the CMS calorimeters. In general, it is expected that the jet quenching effect on partons traversing the medium with different path lengths will lead to modifications in the observed dijet energy balance due to radiated energy which can fall outside the definition of the jet cone. Such unbalanced events are easy to detect visually even at the level of event displays, and numerous examples were in fact seen during the first days of data taking (e.g., Fig. 1).
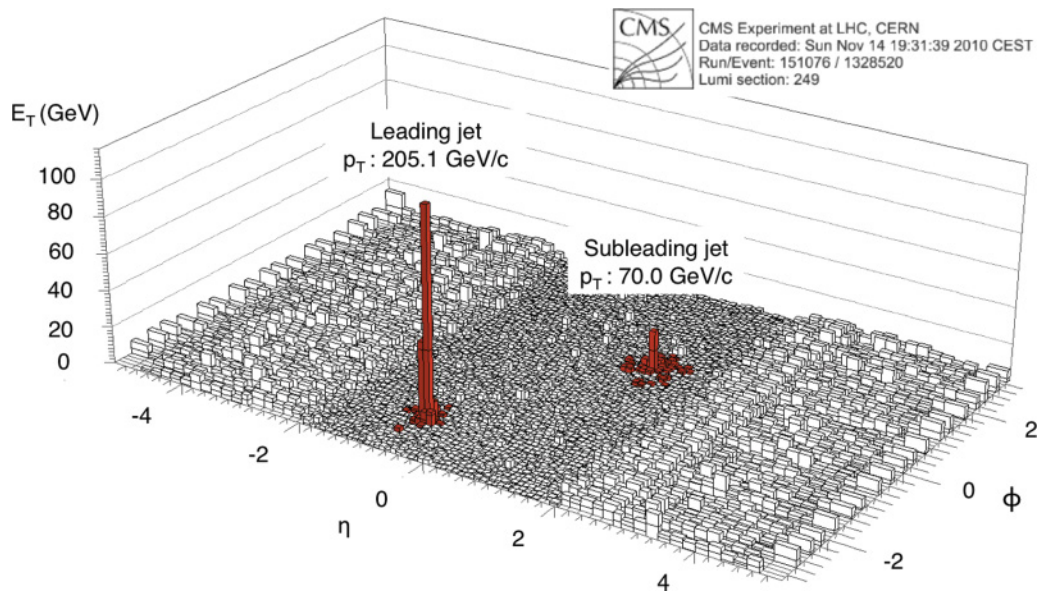

FIG. 1. (Color online) Example of an unbalanced dijet in a PbPb collision event at $\sqrt{s_{NN}} = 2.76$ TeV. Plotted is the summed transverse energy in the electromagnetic and hadron calorimeters vs η and ϕ, with the identified jets highlighted in red, and labeled with the corrected jet transverse momentum.

The data provide information on the evolution of the dijet imbalance as a function of both collision centrality (i.e., the degree of overlap of the two colliding nuclei) and the energy of the leading jet. By correlating the dijets detected in the calorimeters with charged hadrons reconstructed in the high-resolution tracking system, the modification of the jet fragmentation pattern can be studied in detail, thus providing a deeper insight into the dynamics of the jet quenching phenomenon.

The paper is organized as follows: The experimental setup, event triggering, selection and characterization, and jet reconstruction are described in Sec. II. Section III presents the results and a discussion of systematic uncertainties, followed by a summary in Sec. IV.

II. EXPERIMENTAL METHOD

The CMS detector is described in detail elsewhere [29]. The calorimeters provide hermetic coverage over a large range of pseudorapidity $|\eta| < 5.2$, where $\eta = -\ln[\tan(\theta/2)]$ and θ is the polar angle relative to the particle beam. In this study, jets are identified primarily using the energy deposited in the lead-tungstate crystal electromagnetic calorimeter (ECAL) and the brass and scintillator hadron calorimeter (HCAL) covering $|\eta| < 3$. In addition, a steel and quartz-fiber Cherenkov calorimeter, called hadron forward (HF), covers the forward rapidities $3 < |\eta| < 5.2$ and is used to determine the centrality of the PbPb collision. Calorimeter cells are grouped in projective towers of granularity in pseudorapidity and azimuthal angle given by $\Delta\eta \times \Delta\varphi = 0.087 \times 0.087$ at central rapidities, having a coarser segmentation approximately twice as large at forward rapidities. The central calorimeters are embedded in a solenoid with 3.8 T central magnetic field. The event display shown in Fig. 1 illustrates the projective calorimeter

tower granularity over the full pseudorapidity range. The CMS tracking system, located inside the calorimeter, consists of pixel and silicon-strip layers covering $|\eta| < 2.5$, and provides track reconstruction down to $p_T \approx 100$ MeV/c, with a track momentum resolution of $\sim 1\%$ at $p_T = 100$ GeV/c. A set of scintillator tiles, the beam scintillator counters (BSC), are mounted on the inner side of the HF calorimeters for triggering and beam-halo rejection. CMS uses a right-handed coordinate system, with the origin located at the nominal collision point at the center of the detector, the x axis pointing toward the center of the LHC ring, the y axis pointing up (perpendicular to the LHC plane), and the z axis along the counterclockwise beam direction. The detailed Monte Carlo (MC) simulation of the CMS detector response is based on GEANT4 [30].

A. Data samples and triggers

The expected cross section for hadronic inelastic PbPb collisions at $\sqrt{s_{NN}} = 2.76$ TeV is 7.65 b, corresponding to the chosen Glauber MC parameters described in Sec. II C. In addition, there is a sizable contribution from large impact parameter ultra-peripheral collisions (UPCs) that lead to the electromagnetic breakup of one or both of the Pb nuclei [31]. As described later, the few UPC events which pass the online event selection are removed in the offline analysis.

For online event selection, CMS uses a two-level trigger system: level-1 (L1) and high level trigger (HLT). The events for this analysis were selected using an inclusive single-jet trigger that required a L1 jet with $p_T > 30$ GeV/c and a HLT jet with $p_T > 50$ GeV/c, where neither p_T value was corrected for the p_T-dependent calorimeter energy response discussed in Sec. II D. The efficiency of the jet trigger is shown in Fig. 2(a) for leading jets with $|\eta| < 2$ as a function of their corrected p_T. The efficiency is defined as the fraction of triggered events out of a sample of minimum bias events (described below) in bins
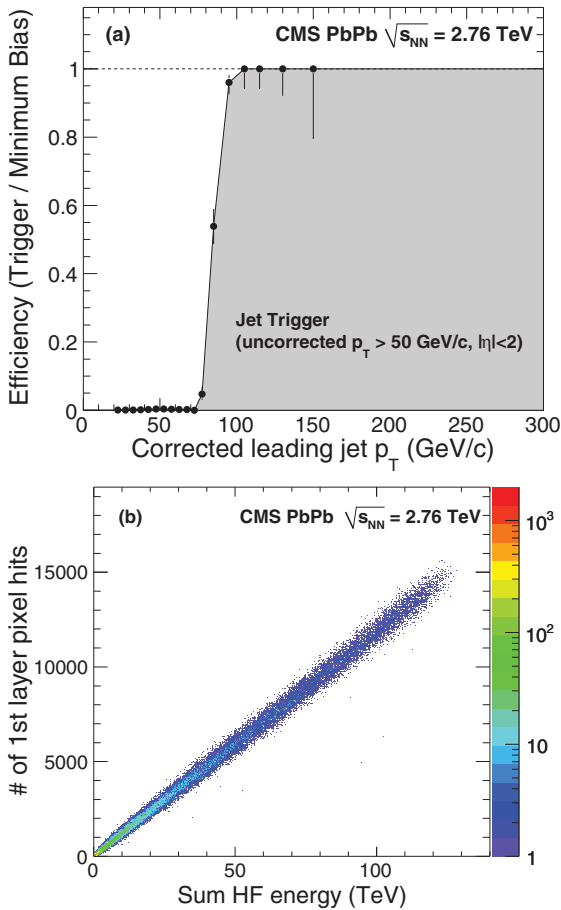
FIG. 2. (Color online) (a) Efficiency curve for the HLT 50 GeV/c single-jet trigger, as a function of the corrected leading jet transverse momentum. Error bars shown are statistical. (b) Correlation between the number of pixel hits and HF total energy for a single run containing 60k minimum bias events, after selections as described in the text.

of offline reconstructed leading jet p_T. The trigger becomes fully efficient for collisions with a leading jet with corrected p_T greater than 100 GeV/c.

In addition to the jet data sample, a minimum bias event sample was collected using coincidences between the trigger signals from the $+z$ and $-z$ sides of either the BSC or the HF. This trigger has an efficiency of more than 97% for hadronic inelastic PbPb collisions. In order to suppress non-collision related noise, cosmic rays, double-firing triggers, and beam backgrounds, the minimum bias and jet triggers used in this analysis were required to fire in time with the presence of both colliding ion bunches in the interaction region. It was checked that the events selected by the jet trigger described above also satisfy all triggers and selections imposed for minimum bias events. The total hadronic collision rate varied between 1 and 210 Hz, depending on the number of colliding bunches (between 1×1 and 129×129) and on the bunch intensity.

B. Event selection

In order to select a pure sample of inelastic hadronic collisions for analysis, a number of offline selections were applied to the triggered event sample, removing contaminations from UPC events and non-collision beam backgrounds (e.g., beam gas). Table I shows the number of events remaining after the various selection criteria are applied. First, beam-halo events were vetoed based on the timing of the $+z$ and $-z$ BSC signals. Then, to veto UPC and beam-gas events, an offline HF coincidence of at least three towers on each side of the interaction point was required, with a total deposited energy of at least 3 GeV. Next, a reconstructed vertex was required with at least two tracks of $p_T > 75$ MeV/c, consistent with the transverse beam spot position and the expected collision region along the z axis. Finally, to further reject beam-gas and beam-scraping events, the length of pixel clusters along the beam direction were required to be compatible with particles originating from the primary vertex. This last selection is identical to the one used for the study of charged hadron pseudorapidity density and p_T spectrum in 7 TeV pp collisions [32]. Figure 2(b) shows the correlation between the total energy deposited in the HF calorimeters and the number of hits in the first layer of the silicon pixel barrel detector after these event selections. A tight correlation between the two detectors is observed, with very few of the events showing HF energy deposits that deviate significantly (at any given number of pixel hits) from the expectations for hadronic PbPb collisions. This correlation is important to verify the selection

TABLE I. Event selection criteria used for this analysis. The percentage of events remaining after each criterion, listed in the last column, are with respect to the previous criterion (the event selection criteria are applied in the indicated sequence).

Criterion	Events remaining	% of events remaining
Jet triggered events ($p_T^{uncorr} > 50$ GeV/c)	149k	100.00
No beam halo, based on the BSC	148k	99.61
HF offline coincidence	111k	74.98
Reconstructed vertex	110k	98.97
Beam-gas removal	110k	99.78
ECAL cleaning	107k	97.66
HCAL cleaning	107k	99.97
$\geqslant 2$ jets with $p_T > 35$ GeV/c and $|\eta| < 2$	71.9k	67.07
Leading jet $p_{T,1} > 120$ GeV/c	4216	5.86
Subleading jet $p_{T,2} > 50$ GeV/c	3684	87.38
$\Delta\phi_{12}$ of 2 jets $> 2\pi/3$	3514	95.39

of a pure collision event sample, and also to validate the HF energy sum as a measure of event centrality (Sec. II C).

Starting from inelastic hadron collisions based on the selections described above, the basic offline selection of events for the analysis is the presence of a leading calorimeter jet in the pseudorapidity range of $|\eta| < 2$ with a corrected jet $p_T > 120$ GeV/c (corrected for the p_T-dependent calorimeter energy response). By selecting these leading jets we avoid possible biases due to inefficiencies close to the trigger threshold. Furthermore, the selection of a rather large leading jet momentum expands the range of jet momentum imbalances that can be observed between the leading and subleading jets, as the subleading jets need a minimum momentum of $p_T > 35$–50 GeV/c to be reliably detected above the high-multiplicity underlying event in PbPb collisions (Sec. II D). In order to ensure high-quality dijet selection, kinematic selection cuts were applied. The azimuthal angle between the leading and subleading jet was required to be at least $2\pi/3$. Also, we require a minimum p_T of $p_{T,1} > 120$ GeV/c for leading jets and of $p_{T,2} > 50$ GeV/c for subleading jets. No explicit requirement is made either on the presence or absence of a third jet in the event. Prior to jet finding on the selected events, a small contamination of noise events from ECAL and HCAL was removed using signal timing, energy distribution, and pulse-shape information [33,34]. As a result, ∼2.4% of the events were removed from the sample.

C. Centrality determination

For the analysis of PbPb events, it is important to know the "centrality" of the collision, i.e., whether the overlap of the two colliding nuclei is large or small. In this analysis, the observable used to determine centrality is the total energy from both HF calorimeters. The distribution of the HF signal used in this analysis is shown in Fig. 3(a). The shape of the energy distribution is characteristic of all observables related to (soft) particle production in heavy-ion collisions. The more frequent peripheral events with a large impact parameter produce very few particles, while the central ones with a small impact parameter produce many more particles because of the increased number of nucleon-nucleon interactions.

The distribution of this total energy was used to divide the event sample into 40 centrality bins, each representing 2.5% of the total nucleus-nucleus interaction cross section. Because of inefficiencies in the minimum bias trigger and event selection, the measured multiplicity distribution does not represent the full interaction cross section. MC simulations were used to estimate the distribution in the regions where events are lost. Comparing the simulated distribution to the measured distribution, it is estimated that the minimum bias trigger and event selection efficiency is $97 \pm 3\%$.

For the jet analysis, these fine-grained bins were combined into five larger bins corresponding to the most central 10% of the events (i.e., smallest impact parameter), the next most central 10% of the events (denoted 10%–20%), and further bins corresponding to the 20%–30%, 30%–50%, and 50%–100% selections of the total hadronic cross section.

Simulations can be used to correlate centrality, as quantified using the fraction of the total interaction cross section, with
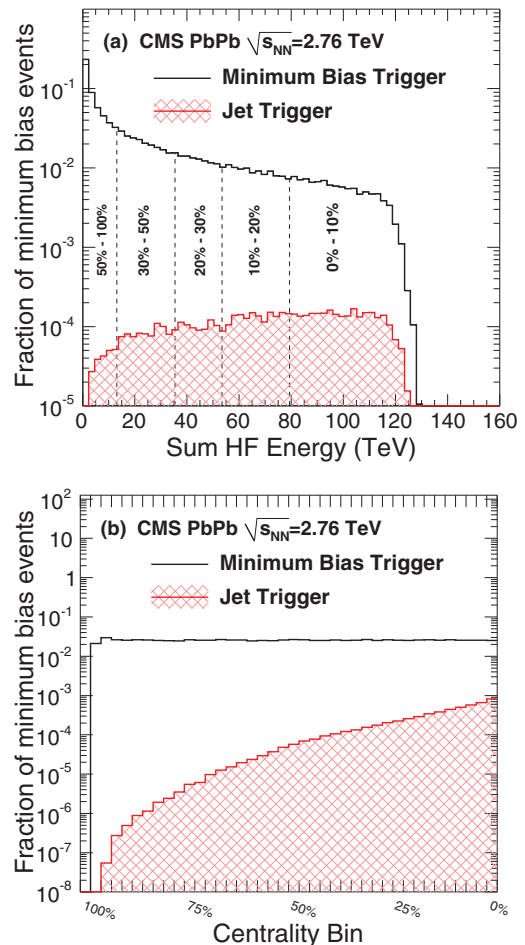

FIG. 3. (Color online) (a) Probability distribution of the total HF energy for minimum bias collisions (black open histogram). The five regions correspond to the centrality ranges used in this analysis. Also shown is the HF energy distribution for the subset of events passing the HLT jet trigger (red hatched histogram). (b) Distribution of the fraction of events in the 40 centrality bins for minimum bias (black open histogram) and HLT jet triggered (red hatched histogram) events. The centrality-bin labels run from 100% for the most peripheral to 0% for the most central events.

more detailed properties of the collision. The two most commonly used physical quantities are the total number of nucleons in the two lead (^{208}Pb) nuclei which experienced at least one inelastic collision, denoted N_{part}, and the total number of binary nucleon-nucleon collisions N_{coll}.

The centrality bins can be correlated to the impact parameter b and to average values and variances of N_{part} and N_{coll} using a calculation based on a Glauber model in which the nucleons are assumed to follow straight-line trajectories as the nuclei collide (for a review, see Ref. [35]). The bin-to-bin smearing of the results of these calculations due to the finite resolution and fluctuations in the HF energy measurement was obtained from fully simulated and reconstructed MC events generated with the AMPT event generator [36]. Standard parameters of the Woods-Saxon function used to model the distribution of nucleons in the Pb nuclei were used [37]. The nucleon-nucleon inelastic cross section, which is used to determine how close

TABLE II. Mean and RMS values for the distributions of impact parameter b, number of participating nucleons N_{part}, and number of nucleon-nucleon collisions N_{coll} for the centrality bins used in this analysis. The rms values represent the spread of each quantity within the given bins due to the range of percentage cross section included.

Centrality	b mean (fm)	b RMS (fm)	N_{part} mean	N_{part} RMS	N_{coll} mean	N_{coll} RMS
0%–10%	3.4 ± 0.1	1.2	355 ± 3	33	1484 ± 120	241
10%–20%	6.0 ± 0.2	0.8	261 ± 4	30	927 ± 82	183
20%–30%	7.8 ± 0.2	0.6	187 ± 5	23	562 ± 53	124
30%–50%	9.9 ± 0.3	0.8	108 ± 5	27	251 ± 28	101
50%–100%	13.6 ± 0.4	1.6	22 ± 2	19	30 ± 5	35

the nucleon trajectories need to be in order for an interaction to occur, was taken to be 64 ± 5 mb, based on a fit of the existing data for total and elastic cross sections in proton-proton and proton-antiproton collisions [38]. The uncertainties in the parameters involved in these calculations contribute to the systematic uncertainty in N_{part} and N_{coll} for a given bin. The other source of uncertainty in the centrality parameters comes from the determination of the event selection efficiency.

Using the procedure outlined above, the mean and spread (RMS) values of the impact parameter N_{part} and N_{coll} for the five bins used in this analysis, and their systematic uncertainties, were extracted and are listed in Table II. The rms values for the centrality parameters are due to their correlation with the percentage cross section and the width of the chosen centrality bins.

It is important to note that the selection of rare processes, such as the production of high-p_T jets, leads to a strong bias in the centrality distribution of the underlying events toward more central collisions, for which N_{coll} is very large. This can be seen in Fig. 3(a), where the HF energy distribution for events selected by the jet trigger is shown in comparison to that for minimum bias events. The bias can be seen more clearly in Fig. 3(b), where the distribution of minimum bias and jet-triggered events in the 40 centrality bins is shown.

D. Jet reconstruction in PbPb collisions

1. Jet algorithm

The baseline jet reconstruction for heavy-ion collisions in CMS is performed with an iterative cone algorithm modified to subtract the soft underlying event on an event-by-event basis [39]. Each cone is selected with a radius $\Delta R = \sqrt{\Delta\phi^2 + \Delta\eta^2} = 0.5$ around a tower cell with the highest-energy deposition with a minimum transverse energy of 1 GeV. The underlying event subtraction algorithm is a variant of an iterative "noise and pedestal subtraction" technique [40]. Initially, the mean value $\langle E_{cell} \rangle$ and dispersion $\sigma(E_{cell})$ of the energies recorded in the calorimeter cells are calculated for all rings of cells that have at least 0.3 GeV transverse energy deposit at constant pseudorapidity. The algorithm subtracts $\langle E_{cell} \rangle + \sigma(E_{cell})$ from each cell. If a cell energy is negative after subtraction, the value is set to zero. Subtracting the mean plus the dispersion, as opposed to simply the mean, compensates for the bias caused by the "zeroing" of negative-energy cells. Jets are then reconstructed, using a standard iterative cone algorithm [41,42], from the remaining cells with nonzero energy. In a second iteration, the pedestal function

is recalculated using only calorimeter cells outside the area covered by reconstructed high-p_T jets ($p_T > 10$ GeV/c). The threshold of 10 GeV/c was chosen in studies optimizing the final extracted jet p_T resolution. The cell energies are updated with the new pedestal function (again subtracting mean plus dispersion) and the jets are reconstructed again, using the updated calorimeter cells. The performance of this algorithm is documented in Ref. [39]. Jet corrections for the calorimeter response have been applied, as determined in studies for pp collisions [43]. When applying the algorithm to PbPb data, the subtracted background energy for $R = 0.5$ jet cones ranges from 6 to 13 GeV for peripheral events (centrality bins 50%–100%) to 90–130 GeV for central collisions (0%–10%), before applying jet energy scale corrections.

To perform a cross check of the main results, the anti-k_T algorithm [44] with a resolution parameter of 0.5 was used to reconstruct jets, as was done for the pp reference measurements presented here. The energy attributed to the underlying event was estimated and subtracted using the "average energy per jet area" procedure provided by the FASTJET package [45,46]. In order to eliminate biases in the underlying event estimation, an η strip of total width $\Delta\eta = 1.6$ centered on the jet position was used, with the two highest-energy jets in each event excluded [47]. In addition, the anti-k_T jets were reconstructed based on particle flow objects [48,49] instead of calorimeter-only information. A good agreement was found with the calorimeter-based, iterative cone algorithm results.

2. Simulated data samples

For the analysis of dijet properties in PbPb events, it is crucial to understand how the jet reconstruction is modified in the presence of the high multiplicity of particles produced in the PbPb underlying event. The jet-finding performance was studied using dijets in pp collisions simulated with the PYTHIA event generator (version 6.423, tune D6T) [50], modified for the isospin content of the colliding nuclei [51]. In order to enhance the number of Pythia dijets in the momentum range studied, a minimum $\hat{p}_T$ selection of 80 GeV/c was used. Lower $\hat{p}_T$ selections, as discussed in Ref. [52], were also investigated and found to agree with the $\hat{p}_T = 80$ GeV/c results within uncertainties. The PYTHIA dijet events were processed with the full detector simulation and analysis chain. Additional samples were produced in which the PYTHIA dijet events were embedded into a minimum bias selection of PbPb events at the raw data level [53]. For this embedding procedure, both real PbPb data events (PYTHIA + DATA), and PbPb events simulated with the HYDJET event generator [51]
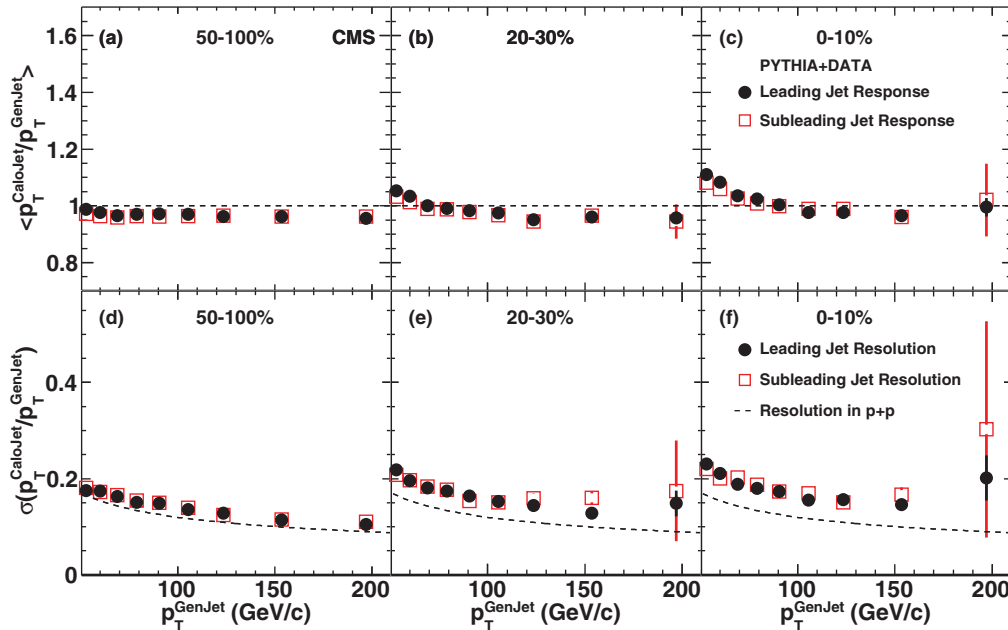
FIG. 4. (Color online) The top row shows the mean of the ratio of reconstructed to generated jet momenta $\langle p_T^{\mathrm{CaloJet}}/p_T^{\mathrm{GenJet}} \rangle$ as a function of p_T^{GenJet}, while the bottom row shows the relative resolution, i.e., the standard deviation of $p_T^{\mathrm{CaloJet}}/p_T^{\mathrm{GenJet}}$. The standard pp jet energy corrections are included in p_T^{CaloJet}. Filled circles are for the leading jets and open squares are for the subleading jets. The left-hand, center, and right-hand columns are for jets in PYTHIA + DATA events with centrality 50%–100%, 20%–30%, and 0%–10%, respectively. On the jet resolution plots (bottom row), the dashed line is a fit to the leading jet resolution in pp events. The vertical bars denote the statistical uncertainty.

(PYTHIA + HYDJET) were used. The HYDJET parameters were tuned to reproduce the total particle multiplicities at all centralities and to approximate the underlying event fluctuations seen in data. The HYDJET events included the simulation of hard-scattering processes for which radiative parton energy loss was simulated, but collisional energy loss was turned off [51]. Both embedded samples were propagated through the standard reconstruction and analysis chain.

The PYTHIA + DATA sample was used in several ways for studies of calorimeter jets. First, by matching the same PYTHIA dijet event reconstructed with and without the PbPb underlying event, the degradation of the jet p_T and position resolution, the jet p_T scale, and the jet-finding efficiency were determined as a function of collision centrality and jet p_T (Sec. II D3). In addition, PYTHIA + DATA events were compared to nonembedded PYTHIA for dijet observables such as azimuthal correlations and momentum balance distributions. Finally, to separate effects due to the medium itself from effects simply due to reconstructing jets in the complicated environment of the underlying PbPb event, a direct comparison of results for PYTHIA + DATA and actual data events was made (Sec. III A).

The PYTHIA + HYDJET sample was used for studies of track momentum balance and track-jet correlations (Secs. III B and III C), where access to the full MC particle level (truth) information for charged tracks is important for systematic studies.

3. Jet-finding performance

A detailed characterization of the CMS calorimeter jet-finding performance in pp collisions can be found in Ref. [54]. The dependence of the jet energy scale and of the jet energy resolution on centrality was determined using the PYTHIA + DATA sample (Fig. 4, standard pp jet energy corrections are applied [43]). In this study, reconstructed jets were matched to the closest generator-level jet in η-ϕ within a cone of $\Delta R = 0.3$. The residual jet energy scale dependence and the relative jet energy resolution are derived from the mean and standard deviation of the Gaussian distributions of the ratio of the reconstructed calorimeter jet transverse momentum p_T^{CaloJet} and the transverse momentum of jets reconstructed based on event generator level final state particles p_T^{GenJet}. For peripheral events in the 50%–100% centrality selection, the jet energies are undercorrected by 5% after applying the standard pp jet energy corrections. The difference between corrected jets reconstructed in PbPb compared to generator jets is the residual jet energy correction, which is not applied, but included in the systematic uncertainty. For the most central events, the large transverse energy per unit area of the underlying event leads to an overcorrection of low-p_T jet energies by up to 10% and a degradation of the relative resolution by $\sim$30% to $\sigma(p_T^{\mathrm{CaloJet}}/p_T^{\mathrm{GenJet}}) = 0.16$ at $p_T = 100$ GeV/c. The jet energy resolution is found to be $\sim$15% worse in central PbPb events than in pp collisions, where the % is with respect to the energy of the generator jet. The effect of the underlying event on the jet angular resolution was also studied. Integrated over jet $p_T > 50$ GeV/c, the angular resolution in ϕ worsens from 0.03 for peripheral events (50%–100%) to 0.04 for central events (0%–10%), while the resolution in η changes from 0.02 to 0.03 over the same centrality range. With the embedding of PYTHIA into minimum bias PbPb data and comparison of reconstructed jets to generator level jets, the effect of the soft
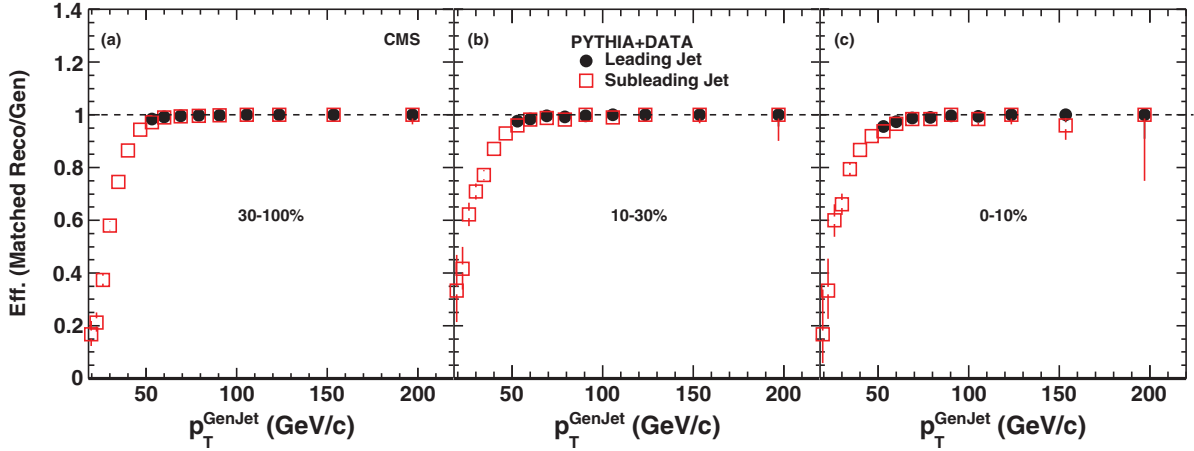
FIG. 5. (Color online) Jet reconstruction efficiency as a function of generator level jet p_T for the leading jet (filled circles) and subleading jet (open squares). From left to right three centrality bins are shown: 30%–100%, 10%–30%, 0%–10%. The vertical bars denote the statistical uncertainty.

heavy-ion background can be understood. The contribution of the background, including fluctuations, was studied both with embedded events, and with random cone studies in minimum bias events for which jets have been reconstructed. For central PbPb events in comparison to pp the degradation of the jet energy resolution caused by the soft background and its fluctuations is 8 ± 2 GeV.

The jet reconstruction efficiency as a function of jet p_T and centrality was extracted from the PYTHIA + DATA sample as well, with the results shown in Fig. 5. For peripheral events, a jet-finding efficiency of 95% was found for a jet $p_T = 50$ GeV/c, while for central collisions the efficiency drops to 88% at the same p_T. Jets with $p_T > 70$ GeV/c are found with an efficiency greater than 97% for all collision centralities. No correction for the inefficiency near the threshold was applied in the subsequent analysis, as the effects of the reconstruction inefficiency are included in the PYTHIA + DATA reference analysis.

Finally, the rate of calorimeter jets reconstructed from fluctuations in the underlying event without the presence of a fragmenting p_T parton, so-called fake jets, for the jet selection used in this paper was determined using fully simulated 0%–10% central HYDJET events. Reconstructed jets in this sample are classified as fake jets if no matching generator-level jet of $p_T > 20$ GeV/c is found within an η-ϕ distance to the reconstructed jet axis smaller than 0.3. For leading jets with $p_{T,1} > 120$ GeV/c, a fake jet fraction of less than 0.02% is found. In events with a $p_{T,1} > 120$ GeV/c leading jet, the fake jet fraction on the away side of the leading jet ($\Delta\phi_{12} > 2\pi/3$) is determined to be 3.5% for reconstructed jets with $p_{T,2} > 50$ GeV/c and less than 0.02% for $p_{T,2} > 120$ GeV/c. The effects of the degradation of jet performance in terms of energy scale, resolution, efficiency, and fake rate on the dijet observables are discussed in Sec. III A.

III. RESULTS

The goal of this analysis is to characterize possible modifications of dijet properties as a function of centrality in PbPb collisions. In addition to the standard event selection of inelastic hadronic collisions and the requirement of a leading jet with $p_{T,1} > 120$ GeV/c (Sec. II B), most of the subsequent analysis required the subleading jet in the event to have $p_{T,2} > 50$ GeV/c, and the azimuthal angle between the leading and subleading jet ($\Delta\phi_{12}$) to be larger than $2\pi/3$. Only jets within $|\eta| < 2$ were considered for the analysis of calorimeter jets in Sec. III A. For a data set of 149k jet events, this selection yields 3514 jet pairs. For studies of correlations of calorimeter jets with charged particles (Secs. III B and III C), a more restrictive pseudorapidity selection was applied. The analysis was performed mostly in five bins of collision centrality: 0%–10%, 10%–20%, 20%–30%, 30%–50%, and 50%–100%.

Thus far, no pp reference data exist at the PbPb collision energy of $\sqrt{s_{NN}} = 2.76$ TeV. Throughout the paper, the results obtained from PbPb data will be compared to references based on the PYTHIA and PYTHIA + DATA samples described in Sec. II D2.

For most results, the PYTHIA + DATA events will be used for direct comparisons. To calibrate the performance of PYTHIA for the observables used in this analysis, the dijet analysis was also performed using the anti-k_T algorithm on 35 pb^{-1} of pp data at $\sqrt{s} = 7$ TeV, collected by CMS prior to the heavy-ion data taking and compared to PYTHIA simulations for the same collision system and energy. The same jet selection criteria used for the 2.76 TeV PbPb data were applied to both pp data and PYTHIA.

A. Dijet properties in pp and PbPb data

The correlation between the transverse momentum of the reconstructed leading and subleading jets in the calorimeters is plotted in Fig. 6. The top row contains PbPb data for peripheral, midcentral, and central events, the second row shows pp jets simulated by PYTHIA and embedded into PbPb data, and the bottom panel shows pp jets from PYTHIA without embedding. One can already observe a downward shift in the subleading jet p_T for the more central PbPb events. In the following discussion, a more quantitative and detailed assessment of this phenomenon will be presented.
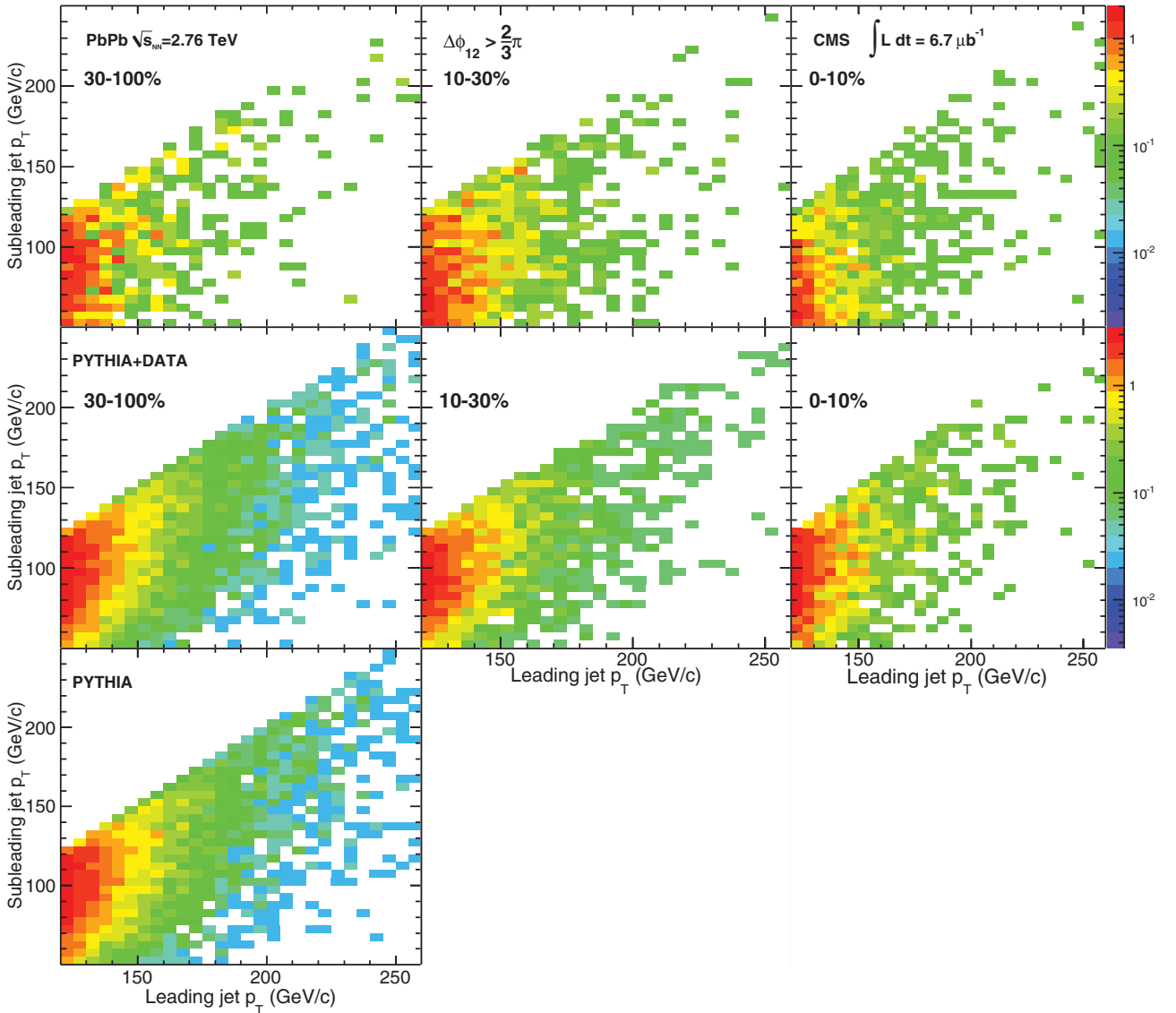
FIG. 6. (Color online) Subleading jet p_T vs leading jet p_T distributions with $\Delta\phi_{12} > 2\pi/3$. The top two rows show results for centrality 30%–100% (left-hand column), 10%–30% (middle column) and 0%–10% (right-hand column), for PbPb data (top row) and reconstructed PYTHIA jets embedded into PbPb data events (middle row). The panel in the bottom row shows the distribution for reconstructed jets from PYTHIA alone.

1. Leading jet spectra

Figure 7(a) shows the leading jet p_T distributions for 7 TeV pp data and corresponding PYTHIA simulations. The distribution of leading jet p_T for PbPb is shown in Figs. 7(b)–7(f) for five different centrality bins. The spectra obtained for PbPb data are shown as solid markers, whereas the hatched histograms show the leading jet spectrum reconstructed from PYTHIA + DATA dijet events. All spectra have been normalized to an integral of unity. The detector-level leading jet spectra in PbPb data and the corresponding results for PYTHIA + DATA samples show good quantitative agreement in all centrality bins over the p_T range studied.

It is important to note that the jet momentum spectra at detector level presented here have not been corrected for smearing due to detector resolution, fluctuations in and out

of the jet cone, or underlying event fluctuations. Therefore, a direct comparison of these spectra to analytical calculations or particle-level generator results is not possible. For the jet asymmetry and dijet $\Delta\phi$ distributions discussed below, the effect of the finite jet energy resolution is estimated using the PYTHIA + DATA events.

2. Dijet azimuthal correlations

One possible medium effect on the dijet properties is a change of the back-to-back alignment of the two partons. This can be studied using the event-normalized differential dijet distribution $(1/N)(dN/d\Delta\phi_{12})$ vs $\Delta\phi_{12}$. Figure 8 shows distributions of $\Delta\phi_{12}$ between leading and subleading jets which pass the respective p_T selections. In Fig. 8(a), the dijet $\Delta\phi_{12}$ distributions are plotted for 7 TeV pp data in comparison
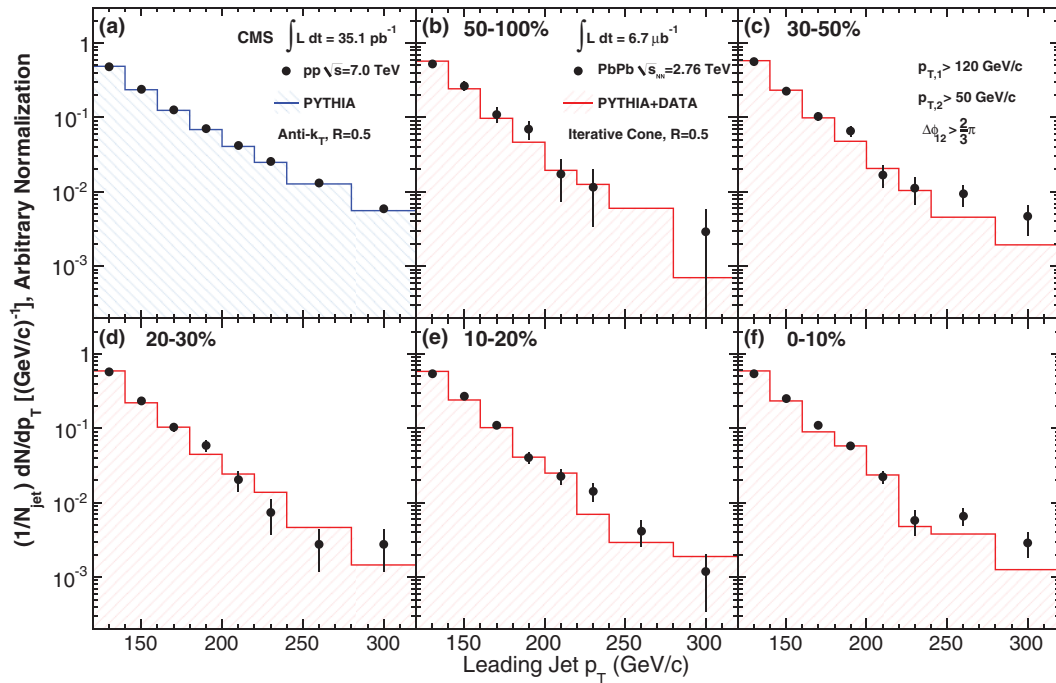
FIG. 7. (Color online) Leading jet p_T distribution for dijet events with subleading jets of $p_{T,2} > 50$ GeV/c and $\Delta\phi_{12} > 2\pi/3$ for 7 TeV pp collisions (a) and 2.76 TeV PbPb collisions in several centrality bins: (b) 50%–100%, (c) 30%–50%, (d) 20%–30%, (e) 10%–20%, and (f) 0%–10%. Data are shown as black points, while the histograms show (a) PYTHIA events and (b)–(f) PYTHIA events embedded into PbPb data. The error bars show the statistical uncertainties.

to the corresponding PYTHIA simulations using the anti-k_T algorithm for jets based on calorimeter information. PYTHIA provides a good description of the experimental data, with

slightly larger tails seen in the PYTHIA simulations. A recent study of azimuthal correlations in pp collisions at 7 TeV can be found in Ref. [55]. For the PYTHIA comparison to
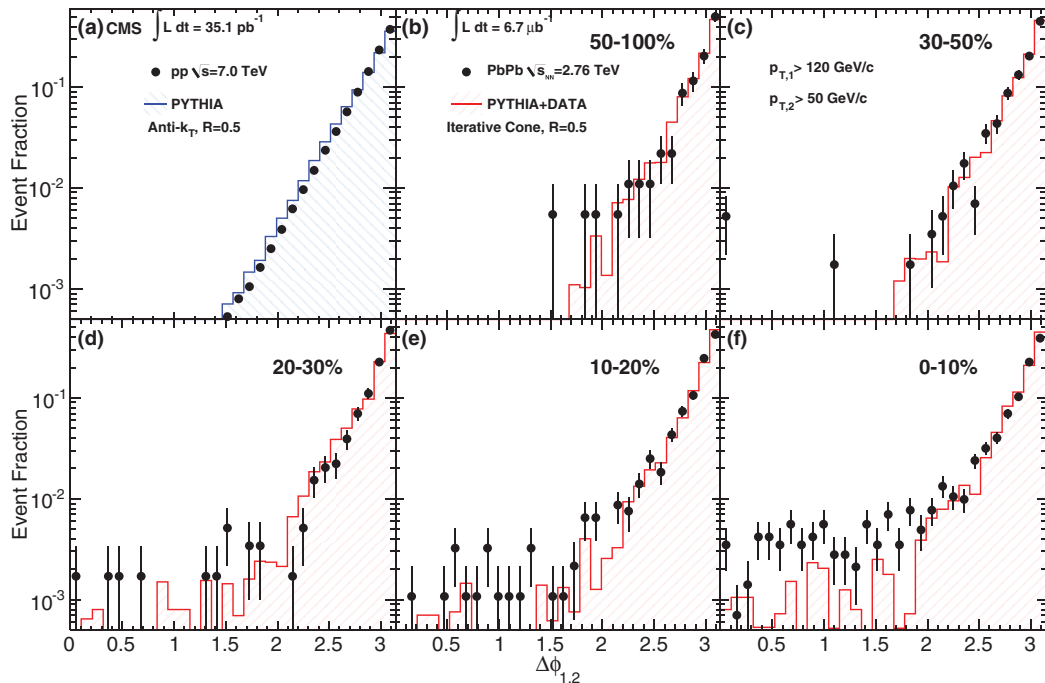
FIG. 8. (Color online) $\Delta\phi_{12}$ distributions for leading jets of $p_{T,1} > 120$ GeV/c with subleading jets of $p_{T,2} > 50$ GeV/c for 7 TeV pp collisions (a) and 2.76 TeV PbPb collisions in several centrality bins: (b) 50%–100%, (c) 30%–50%, (d) 20%–30%, (e) 10%–20%, and (f) 0%–10%. Data are shown as black points, while the histograms show (a) PYTHIA events and (b)–(f) PYTHIA events embedded into PbPb data. The error bars show the statistical uncertainties.
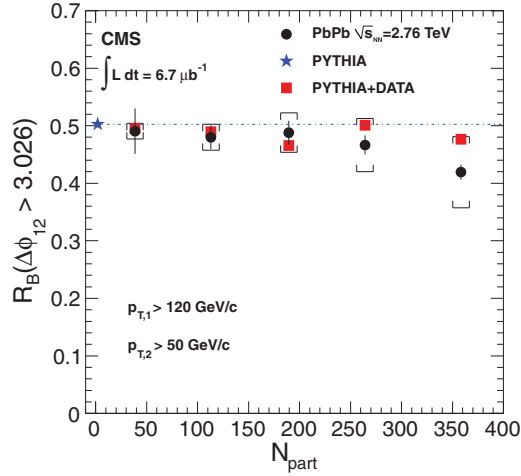
FIG. 9. (Color online) Fraction of events with $\Delta\phi_{12} > 3.026$ as a function of N_{part}, among events with $p_{T,1} > 120$ GeV/c and $p_{T,2} > 50$ GeV/c. The result for reconstructed PYTHIA dijet events (blue filled star) is plotted at $N_{part} = 2$. The other points (from left to right) correspond to centrality bins of 50%–100%, 30%–50%, 20%–30%, 10%–20%, and 0%–10%. The red squares are for reconstruction of PYTHIA + DATA events and the filled circles are for the PbPb data, with statistical (vertical bars) and systematic (brackets) uncertainties.

PbPb results at $\sqrt{s_{NN}} = 2.76$ TeV, this discrepancy seen in the higher-energy pp comparison is included in the systematic uncertainty estimation. It is important to note that the PYTHIA simulations include events with more than two jets, which provide the main contribution to events with large momentum imbalance or $\Delta\phi_{12}$ far from π.

Figures 8(b)–8(f) show the dijet $\Delta\phi_{12}$ distributions for PbPb data in five centrality bins, compared to PYTHIA + DATA simulations. The distributions for the four more peripheral bins are in good agreement with the PYTHIA + DATA reference, especially for $\Delta\phi_{12} \gtrsim 2$. The three centrality bins spanning 0%–30% show an excess of events with azimuthally misaligned dijets ($\Delta\phi_{12} \lesssim 2$), compared with more peripheral events. A similar trend is seen for the PYTHIA + DATA simulations, although the fraction of events with azimuthally misaligned dijets is smaller in the simulation. The centrality dependence of the azimuthal correlation in PYTHIA + DATA can be understood as the result of the increasing fake-jet rate and the drop in jet reconstruction efficiency near the 50 GeV/c threshold from 95% for peripheral events to 88% for the most central events. In PbPb data, this effect is magnified since low-p_T away-side jets can undergo a sufficiently large energy loss to fall below the 50 GeV/c selection criteria.

Furthermore, a reduction of the fraction of back-to-back jets above $\Delta\phi_{12} \gtrsim 3$ is observed for the most central bin. This modification of the $\Delta\phi_{12}$ distribution as a function of centrality can be quantified using the fraction R_B of dijets with $\Delta\phi_{12} > 3.026$, as plotted in Fig. 9, for $p_{T,1} > 120$ GeV/c and $p_{T,2} > 50$ GeV/c. The threshold of 3.026 corresponds to the median of the $\Delta\phi_{12}$ distribution for PYTHIA (without embedding). The results for both the PbPb data and PYTHIA + DATA dijets are shown as a function of the reaction centrality, given by the number of participating nucleons N_{part}, as described in Sec. II C. This observable is not sensitive to the shape of the tail at $\Delta\phi_{12} < 2$ seen in Fig. 8, but can be used to measure small changes in the back-to-back correlation between dijets. A decrease in the fraction of back-to-back jets
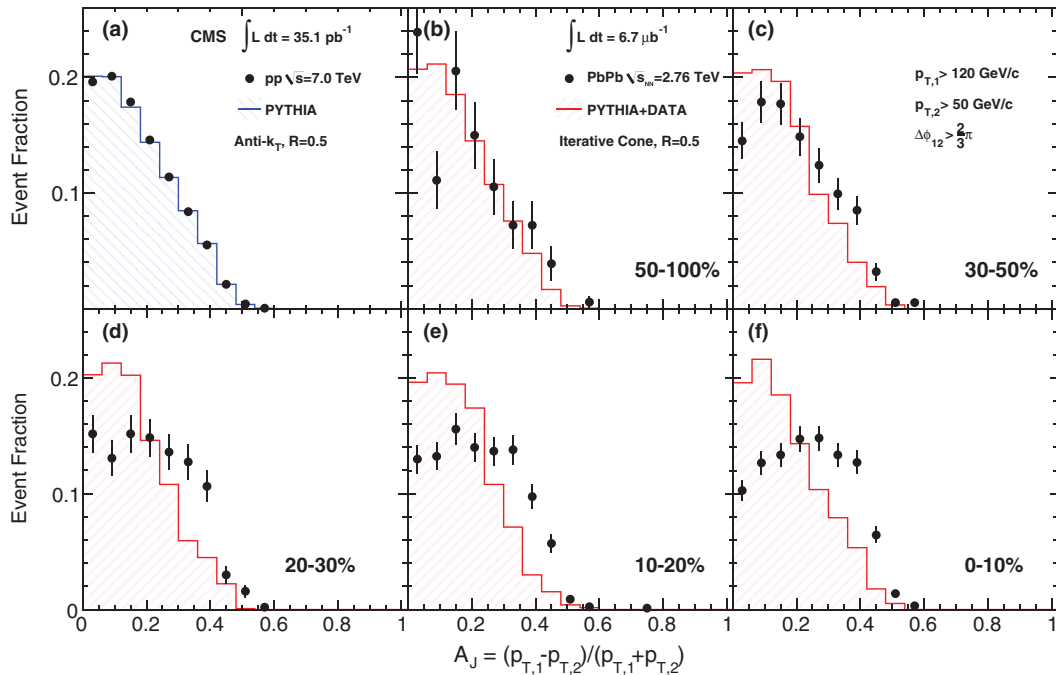

FIG. 10. (Color online) Dijet asymmetry ratio A_J for leading jets of $p_{T,1} > 120$ GeV/c, subleading jets of $p_{T,2} > 50$ GeV/c, and $\Delta\phi_{12} > 2\pi/3$ for 7 TeV pp collisions (a) and 2.76 TeV PbPb collisions in several centrality bins: (b) 50%–100%, (c) 30%–50%, (d) 20%–30%, (e) 10%–20%, and (f) 0%–10%. Data are shown as black points, while the histograms show (a) PYTHIA events and (b)–(f) PYTHIA events embedded into PbPb data. The error bars show the statistical uncertainties.

FIG. 11. (Color online) Fraction of all events with a leading jet with $p_{T,1} > 120$ GeV/c for which a subleading jet with $A_J < 0.15$ and $\Delta\phi_{12} > 2\pi/3$ was found, as a function of $N_{\rm part}$. The result for reconstructed PYTHIA dijet events (blue filled star) is plotted at $N_{\rm part} = 2$. The other points (from left to right) correspond to centrality bins of 50%–100%, 30%–50%, 20%–30%, 10%–20%, and 0%–10%. 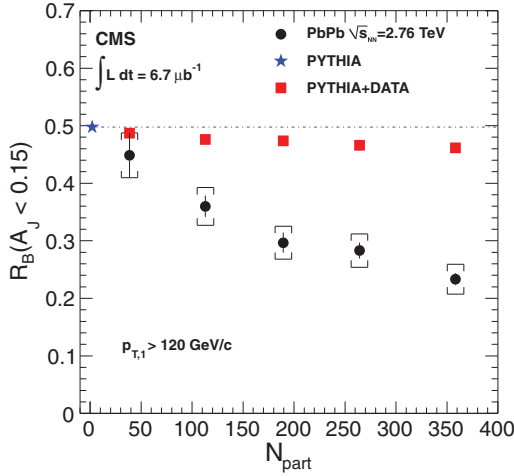The red squares are for reconstruction of PYTHIA + DATA events and the filled circles are for the PbPb data, with statistical (vertical bars) and systematic (brackets) uncertainties.

in PbPb data is seen compared to the pure PYTHIA simulations. Part of the observed change in $R_B(\Delta\phi)$ with centrality is explained by the decrease in jet azimuthal angle resolution from $\sigma_\phi = 0.03$ in peripheral events to $\sigma_\phi = 0.04$ in central events, due to the impact of fluctuations in the PbPb underlying event. This effect is demonstrated by the comparison of PYTHIA and PYTHIA + DATA results. The difference between the pp and PYTHIA + DATA resolutions was used for the uncertainty estimate, giving the dominant contribution to the systematic uncertainties, shown as brackets in Fig. 9.

3. Dijet momentum balance

To characterize the dijet momentum balance (or imbalance) quantitatively, we use the asymmetry ratio

$$A_J = \frac{p_{T,1} - p_{T,2}}{p_{T,1} + p_{T,2}}, \qquad (1)$$

where the subscript 1 always refers to the leading jet, so that A_J is positive by construction. The use of A_J removes uncertainties due to possible constant shifts of the jet energy scale. It is important to note that the subleading jet $p_{T,2} > 50$ GeV/c selection imposes a $p_{T,1}$-dependent limit on the magnitude of A_J. For example, for the most frequent leading jets near the 120 GeV/c threshold, this limit is $A_J < 0.41$, while the largest possible A_J for the present dataset is 0.7 for 300 GeV/c leading jets. Dijets in which the subleading jet is lost below the 50 GeV/c threshold are not included in the A_J calculation. Dijets are selected with $\Delta\phi_{12} > 2\pi/3$

In Fig. 10(a), the A_J dijet asymmetry observable calculated by PYTHIA is compared to pp data at $\sqrt{s} = 7$ TeV. Again, the data and event generator are found to be in agreement [56]. This observation, as well as the good agreement between PYTHIA +

DATA and the most peripheral PbPb data shown in Fig. 10(b), suggest that PYTHIA at $\sqrt{s} = 2.76$ TeV can serve as a good reference for the dijet imbalance analysis in PbPb collisions.

The centrality dependence of A_J for PbPb collisions can be seen in Figs. 10(b)–10(f), in comparison to PYTHIA + DATA simulations. Whereas the dijet angular correlations show only a small dependence on collision centrality, the dijet momentum balance exhibits a dramatic change in shape for the most central collisions. In contrast, the PYTHIA simulations only exhibit a modest broadening, even when embedded in the highest multiplicity PbPb events.

Central PbPb events show a significant deficit of events in which the momenta of leading and subleading jets are balanced and a significant excess of unbalanced pairs. The large excess of unbalanced compared to balanced dijets explains why this effect was apparent even when simply scanning event displays (see Fig. 1). The striking momentum imbalance is also confirmed when studying high-p_T tracks associated with leading and subleading jets, as will be shown in Sec. III B. This observation is consistent with the expected degradation of the parton energy, or jet quenching, in the medium produced in central PbPb collisions [17].

The evolution of the dijet momentum balance illustrated in Fig. 10 can be explored more quantitatively by studying the fraction of balanced jets in the PbPb events. The balanced fraction $R_B(A_J < 0.15)$ is plotted as a function of collision centrality (again in terms of $N_{\rm part}$) in Fig. 11. It is defined as the fraction of all events with a leading jet having $p_{T,1} > 120$ GeV/c for which a subleading partner with $A_J < 0.15$ and $\Delta\phi_{12} > 2\pi/3$ is found. Since $R_B(A_J < 0.15)$ is calculated as the fraction of all events with $p_{T,1} > 120$ GeV/c, it takes into account the rate of apparent "monojet" events, where the subleading partner is removed by the p_T or $\Delta\phi$ selection.

The A_J threshold of 0.15 corresponds to the median of the A_J distribution for pure PYTHIA dijet events passing the criteria used for Fig. 10. By definition, the fraction $R_B(A_J < 0.15)$ of balanced jets in PYTHIA is therefore 50%, which is plotted as a dashed line in Fig. 11. As will be discussed in Sec. III C, a third jet having a significant impact on the dijet imbalance is present in most of the large-A_J events in PYTHIA.

The change in jet-finding performance from high to low p_T, discussed in Sec. II D3, leads to only a small decrease in the fraction of balanced jets, of less than 5% for central PYTHIA + DATA dijets. In contrast, the PbPb data show a rapid decrease in the fraction of balanced jets with collision centrality. While the most peripheral selection shows a fraction of balanced jets of close to 45%, this fraction drops by close to a factor of 2 for the most central collisions. This again suggests that the passage of hard-scattered partons through the environment created in PbPb collisions has a significant impact on their fragmentation into final-state jets.

The observed change in the fraction of balanced jets as a function of centrality, shown in Fig. 11, is far bigger than the estimated systematic uncertainties, shown as brackets. The main contributions to the systematic uncertainties include the uncertainties on jet energy scale and resolution, jet reconstruction efficiency, and the effects of underlying event subtraction. The uncertainty in the subtraction procedure is estimated based on the difference between pure PYTHIA and
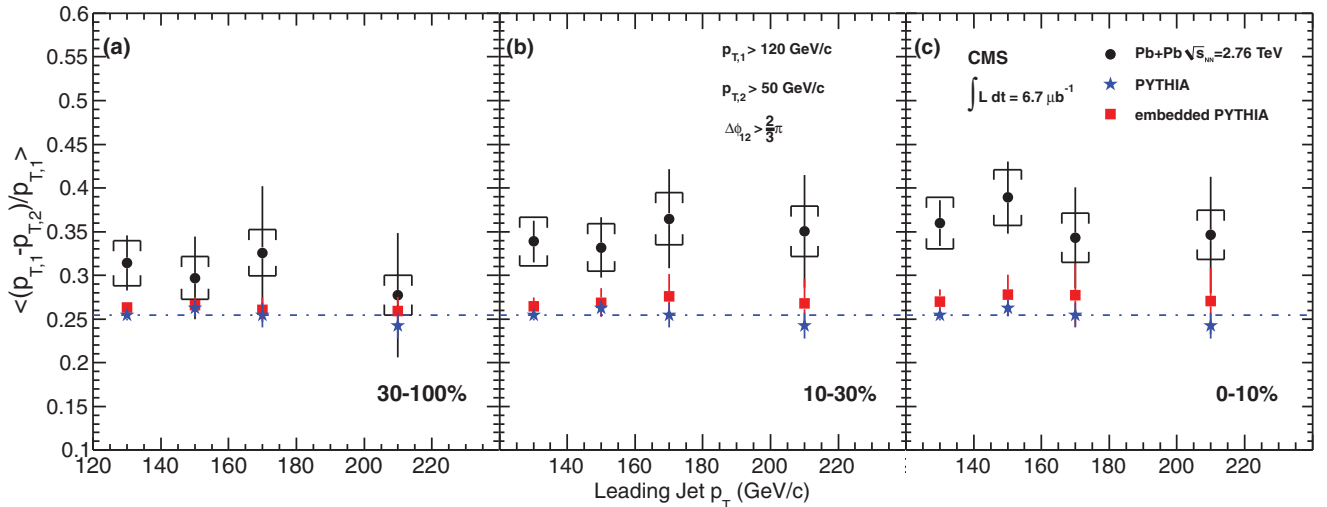
FIG. 12. (Color online) Mean value of the fractional imbalance $(p_{T,1} - p_{T,2})/p_{T,1}$ as a function of leading jet p_T for three centrality bins. The PbPb data are shown as circles with vertical bars and brackets indicating the statistical and systematic uncertainties, respectively. Results for PYTHIA are shown with blue stars, and PYTHIA + DATA with red squares. The dotted-dashed line to guide the eye is drawn at the value for pure PYTHIA for the lowest p_T bin.

PYTHIA + DATA simulations. For central events, the subtraction procedure contributes the biggest uncertainty to $R_B(A_J)$, of close to 8%. The uncertainty on the residual jet energy scale was estimated based on the results shown in the top row of Fig. 4. The full difference between the observed residual correction and unity, added in quadrature with the systematic uncertainty obtained for pp [43], was used as the systematic uncertainty on the jet p_T and propagated to $R_B(A_J)$. For the jet p_T resolution uncertainty, the full difference of the PYTHIA + DATA result to the pp resolution, as shown in Fig. 4 (bottom), was used as an uncertainty estimate for the PbPb jet p_T resolution. The uncertainties in jet energy scale and jet resolution contribute 5% and 6%, respectively, to the 11% total systematic uncertainty in central events. For peripheral events, the total uncertainty drops to 9%, mostly due to the smaller uncertainty related to the PbPb background fluctuations for lower multiplicity events.

4. Leading jet p_T dependence of dijet momentum imbalance

The dependence of the jet modification on the leading jet momentum can be studied using the fractional imbalance $(p_{T,1} - p_{T,2})/p_{T,1}$. The mean value of this fraction is presented as a function of $p_{T,1}$ in Fig. 12 for three bins of collision centrality, 30%–100%, 10%–30%, and 0%–10%. PYTHIA is shown as stars, PYTHIA + DATA simulations are shown as squares, while the data are shown as circles. Statistical and systematic uncertainties are plotted as error bars and brackets, respectively. The dominant contribution to the systematic uncertainty comes from the observed p_T dependence of the residual jet energy correction in PbPb events (6% out of a total systematic uncertainty of 8%). The jet energy resolution and underlying event subtraction uncertainties contribute ~4% each.

The fractional imbalance exhibits several important features: The imbalance seen in PbPb data grows with collision centrality and reaches a much larger value than in PYTHIA or PYTHIA + DATA. In addition, the effect is clearly visible even

for the highest-p_T jets observed in the data set, demonstrating that the observed dijet imbalance is not restricted to the threshold region in our leading jet selection. Within the present uncertainties, the $p_{T,1}$ dependence of the excess imbalance above the PYTHIA prediction is compatible with either a constant difference or a constant fraction of $p_{T,1}$.

The main contributions to the systematic uncertainty in $(p_{T,1} - p_{T,2})/p_{T,1}$ are the uncertainties in the p_T-dependent residual energy scale (based on results shown in the top row of Fig. 4), and the centrality-dependent difference observed between PYTHIA and PYTHIA + DATA seen in Fig. 12. As before, the uncertainty on the residual jet energy scale was estimated using the full difference between the observed residual correction and unity, and also assuming that within these limits the low-p_T and high-p_T response could vary independently.

B. Track-jet correlations

The studies of calorimeter jets show a strong change of the jet momentum balance as a function of collision centrality. This implies a corresponding modification in the distribution of jet fragmentation products, with energy being either transported out of the cone area used to define the jets, or to low-momentum particles which are not measured in the calorimeter jets. The CMS calorimeter is less sensitive to these low momentum particles as they do not reach the calorimeter surface due to the high magnetic field. Information about changes to the effective fragmentation pattern as a function of A_J can be obtained from track-jet correlations. For this analysis, PYTHIA + HYDJET simulations are used as a MC reference, to allow full access to MC truth (i.e., the output of the generator) information for tracks in the dijet signal and in the PbPb underlying event. The event selection for PYTHIA + HYDJET was based on reconstructed calorimeter jet information, as for the previous studies.

To derive the associated track spectrum for a given jet selection in data, the p_T distribution of tracks inside an annulus
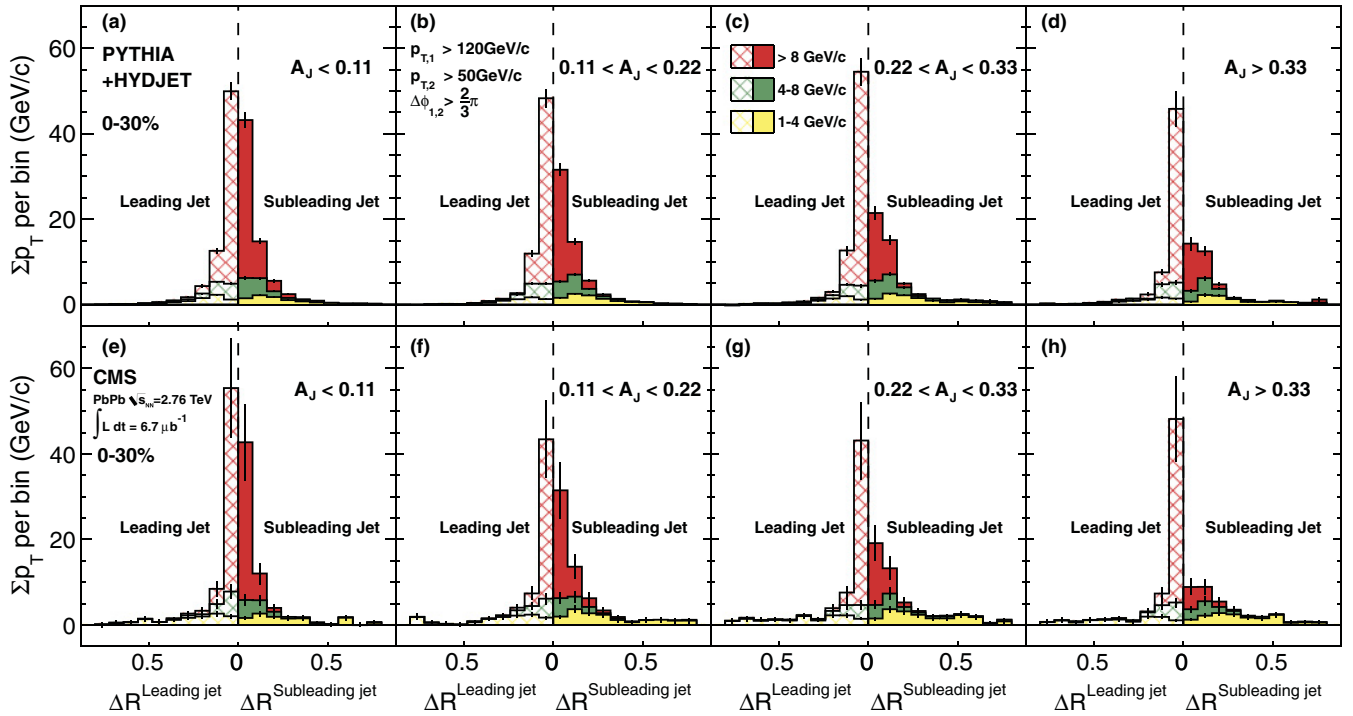
FIG. 13. (Color online) Distribution of the transverse momentum sum of tracks for three p_T ranges, as a function of the distance ΔR to the leading and subleading jet axes. Results for the 0%–30% centrality selection are shown for PYTHIA + HYDJET (upper row) and PbPb data (lower row). For each figure, the requirements on the dijet asymmetry A_J are given. Note that events with $A_J > 0.22$ are much rarer in the PYTHIA+HYDJET sample than in the data. Vertical bars are statistical and systematic uncertainties, combined in quadrature, the systematic contributions being 20%, independent of the bin.

of radius $\Delta R = \sqrt{\Delta\phi^2 + \Delta\eta^2}$ and width of 0.08 around the jet axes was summed over all selected jets. The contribution of tracks from the underlying event, not associated with the jet, was estimated by summing the track p_T distributions using an equal-size annulus that was reflected around $\eta = 0$, but at the same ϕ coordinate as the individual jet. For this procedure, jets in the region $|\eta| < 0.8$ were excluded and only annulus radii up to $\Delta R = 0.8$ around the jet axes were considered, to avoid overlap between the signal jet region and the region used for background estimation. In addition, jets in the region $|\eta| > 1.6$ were excluded to ensure the 0.8 radius rings would lie within the tracker acceptance. Statistical fluctuations in the underlying event limit this procedure to tracks with transverse momenta $p_T > 1$ GeV/c.

The summed p_T spectra from the underlying event regions were then subtracted from the jet regions, yielding the momentum distribution of charged tracks associated with the jets as a function of ΔR.

The resulting distributions of associated track momentum as a function of track p_T and ΔR are presented in Fig. 13 for four selections in dijet asymmetry, from $A_J < 0.11$ (left-hand side) to $A_J > 0.33$ (right-hand side). For both data and PYTHIA + HYDJET results, the jet selections and A_J values are based on the reconstructed calorimeter jet momenta (Sec. II D) in order to have consistent event selections for comparison. The middle bin boundary ($A_J = 0.22$) corresponds to the median of the A_J distribution for the 0%–30% central PbPb events shown here. The top row shows the results for PYTHIA + HYDJET

simulations. The track results shown for the PYTHIA + HYDJET simulations were found using the known ("truth") values of the track momenta from the embedded PYTHIA events. The bottom row presents results for PbPb data. The track results shown for PbPb data were corrected for tracking efficiency and fake rates using corrections that were derived from PYTHIA + HYDJET simulations and from the reconstruction of single tracks embedded in data. In each panel, the area of each colored region in p_T and ΔR corresponds to the total transverse momentum per event carried by tracks in this region.

For the balanced-jet selection $A_J < 0.11$, one sees qualitative agreement in the leading and subleading jet momentum distributions between PYTHIA+HYDJET (top) and data (bottom). In data and simulation, most of the leading and subleading jet momentum is carried by tracks with $p_T > 8$ GeV/c, with the data tracks having a slightly narrower ΔR distribution. A slightly larger fraction of the momentum for the subleading jets is carried by tracks at low p_T and $\Delta R > 0.16$ (i.e., beyond the second bin) in the data.

Moving toward larger dijet imbalance, the major fraction of the leading jet momentum continues to be carried by high-p_T tracks in data and simulation. For the $A_J > 0.33$ selection, it is important to recall that less than 10% of all PYTHIA dijet events fall in this category, and, as will be discussed in Sec. III C, those that do are overwhelmingly 3-jet events.

While the overall change found in the leading jet shapes as a function of A_J is small, a strong modification of

the track momentum composition of the subleading jets is seen, confirming the calorimeter determination of the dijet imbalance. The biggest difference between data and simulation is found for tracks with $p_T < 4$ GeV/c. For PYTHIA, the momentum in the subleading jet carried by these tracks is small and their radial distribution is nearly unchanged with A_J. However, for data, the relative contribution of low-p_T tracks grows with A_J, and an increasing fraction of those tracks is observed at large distances to the jet axis, extending out to $\Delta R = 0.8$ (the largest angular distance to the jet in this study).

The major systematic uncertainties for the track-jet correlation measurement come from the p_T-dependent uncertainty in the track reconstruction efficiency. The algorithmic track reconstruction efficiency, which averages 70% over the $p_T > 0.5$ GeV/c and $|\eta| < 2.4$ range included in this study, was determined from an independent PYTHIA + HYDJET sample, and from simulated tracks embedded in data. Additional uncertainties are introduced by the underlying event subtraction procedure. The latter was studied by comparing the track-jet correlations seen in pure PYTHIA dijet events for generated particles with those seen in PYTHIA + HYDJET events after reconstruction and background subtraction. The size of the background subtraction systematic uncertainty was further cross checked in data by repeating the procedure for random ring-like regions in 0%–30% central minimum bias events. In the end, an overall systematic uncertainty of 20% per bin

was assigned. This uncertainty is included in the combined statistical and systematic uncertainties shown in Fig. 13.

C. Overall momentum balance of dijet events

The requirements of the background subtraction procedure limit the track-jet correlation study to tracks with $p_T > 1.0$ GeV/c and $\Delta R < 0.8$. Complementary information about the overall momentum balance in the dijet events can be obtained using the projection of missing p_T of reconstructed charged tracks onto the leading jet axis. For each event, this projection was calculated as

$$\not{p}_T^{\parallel} = \sum_i -p_T^i \cos(\phi_i - \phi_{\text{Leading Jet}}), \qquad (2)$$

where the sum is over all tracks with $p_T > 0.5$ GeV/c and $|\eta| < 2.4$. The results were then averaged over events to obtain $\langle \not{p}_T^{\parallel} \rangle$. No background subtraction was applied, which allows this study to include the $|\eta_{\text{jet}}| < 0.8$ and $0.5 < p_T^{\text{Track}} < 1.0$ GeV/c regions not accessible for the study in Sec. III B. The leading and subleading jets were again required to have $|\eta| < 1.6$.

In Fig. 14, $\langle \not{p}_T^{\parallel} \rangle$ is shown as a function of A_J for two centrality bins, 30%–100% (left-hand side) and 0%–30% (right-hand side). Results for PYTHIA + HYDJET are presented in the top row, while the bottom row shows the results for PbPb data. Using tracks with $|\eta| < 2.4$ and $p_T > 0.5$ GeV/c, one

FIG. 14. (Color online) Average missing transverse momentum $\langle \not{p}_T^{\parallel} \rangle$ for tracks with $p_T > 0.5$ GeV/c, projected onto the leading jet axis (solid circles). The $\langle \not{p}_T^{\parallel} \rangle$ values are shown as a function of dijet asymmetry A_J for 30%–100% centrality (left-hand side) and 0%–30% centrality (right-hand side). For the solid circles, vertical bars and brackets represent the statistical and systematic uncertainties, respectively. Colored bands show the contribution to $\langle \not{p}_T^{\parallel} \rangle$ for five ranges of track p_T. The top and bottom rows show results for PYTHIA + HYDJET and PbPb data, respectively. For the individual p_T ranges, the statistical uncertainties are shown as vertical bars.

sees that indeed the momentum balance of the events, shown as solid circles, is recovered within uncertainties, for both centrality ranges and even for events with large observed dijet asymmetry, in both data and simulation. This shows that the dijet momentum imbalance is not related to undetected activity in the event due to instrumental (e.g., gaps or inefficiencies in the calorimeter) or physics (e.g., neutrino production) effects.

The figure also shows the contributions to $\langle \not{p}_T^{\parallel} \rangle$ for five transverse momentum ranges from 0.5–1 GeV/c to $p_T >$ 8 GeV/c. The vertical bars for each range denote statistical uncertainties. For data and simulation, a large negative contribution to $\langle \not{p}_T^{\parallel} \rangle$ (i.e., in the direction of the leading jet) by the $p_T > 8$ GeV/c range is balanced by the combined contributions from the 0.5–8 GeV/c regions. Looking at the $p_T < 8$ GeV/c region in detail, important differences between data and simulation emerge. For PYTHIA + HYDJET both centrality ranges show a large balancing contribution from the intermediate p_T region of 4–8 GeV/c, while the contribution from the two regions spanning 0.5–2 GeV/c is very small. In peripheral PbPb data, the contribution of 0.5–2 GeV/c tracks relative to that from 4–8 GeV/c tracks is somewhat enhanced compared to the simulation. In central PbPb events, the relative contribution of low and intermediate-p_T tracks is actually the opposite of that seen in PYTHIA + HYDJET. In data, the 4–8 GeV/c region makes almost no contribution to the overall momentum balance, while a large fraction of the negative imbalance from high p_T is recovered in low-momentum tracks.

The dominant systematic uncertainty for the p_T balance measurement comes from the p_T-dependent uncertainty in the track reconstruction efficiency and fake rate described in Sec. III B. A 20% uncertainty was assigned to the final result, stemming from the residual difference between the PYTHIA generator level and the reconstructed PYTHIA + HYDJET tracks at high p_T. This is combined with an absolute 3 GeV/c uncertainty that comes from the imperfect cancellation of the background tracks. The background effect was cross checked in data from a random cone study in 0%–30% central events similar to the study described in Sec. III B. The overall systematic uncertainty is shown as brackets in Figs. 14 and 15.

Further insight into the radial dependence of the momentum balance can be gained by studying $\langle \not{p}_T^{\parallel} \rangle$ separately for tracks inside cones of size $\Delta R = 0.8$ around the leading and subleading jet axes, and for tracks outside of these cones. The results of this study for central events are shown in Fig. 15 for the in-cone balance and out-of-cone balance for MC and data. As the underlying PbPb event in both data and MC is not ϕ symmetric on an event-by-event basis, the back-to-back requirement was tightened to $\Delta\phi_{12} > 5\pi/6$ for this study.

One observes that for both data and MC an in-cone imbalance of $\langle \not{p}_T^{\parallel} \rangle \approx -20$ GeV/c is found for the $A_J > 0.33$ selection. In both cases this is balanced by a corresponding out-of-cone imbalance of $\langle \not{p}_T^{\parallel} \rangle \approx 20$ GeV/c. However, in the PbPb data the out-of-cone contribution is carried almost entirely by tracks with $0.5 < p_T < 4$ GeV/c, whereas in MC
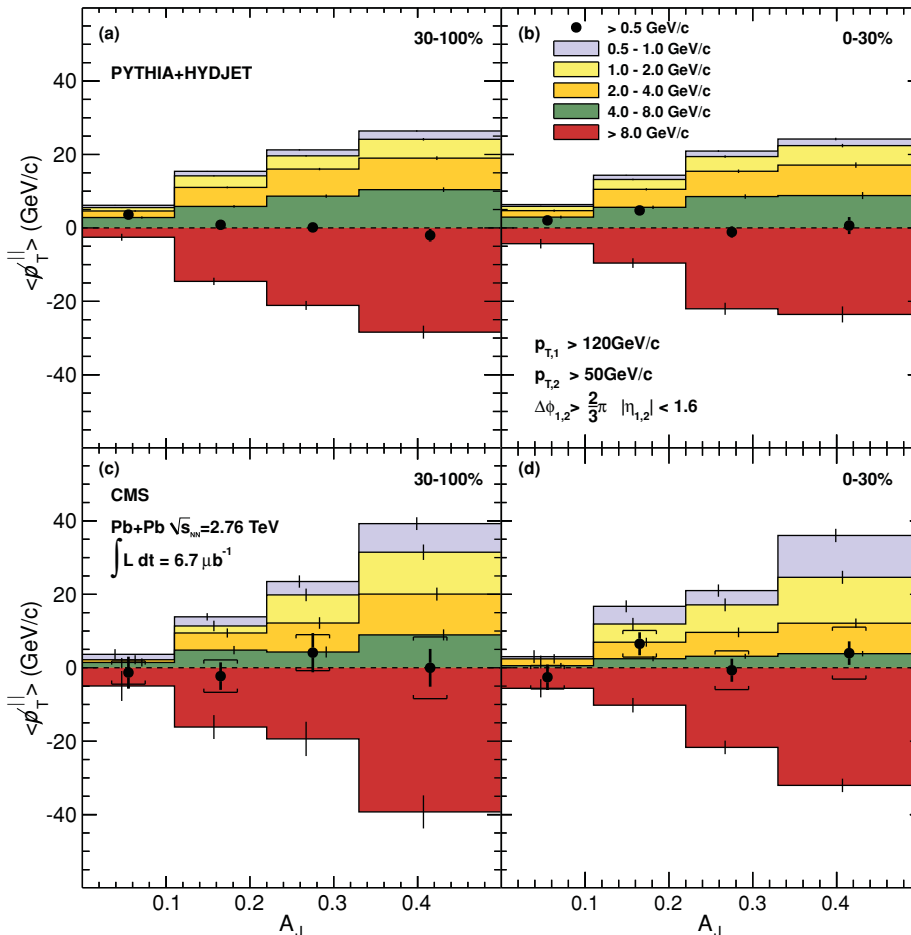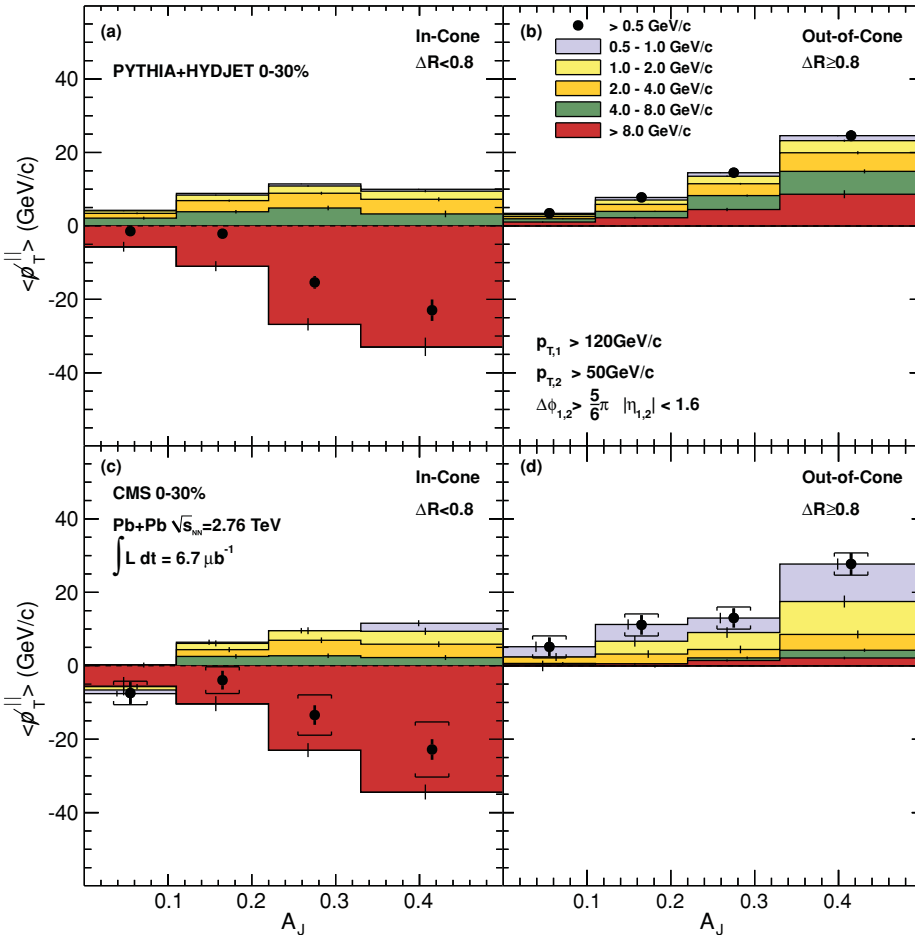

FIG. 15. (Color online) Average missing transverse momentum $\langle \not{p}_T^{\parallel} \rangle$ for tracks with $p_T > 0.5$ GeV/c, projected onto the leading jet axis (solid circles). The $\langle \not{p}_T^{\parallel} \rangle$ values are shown as a function of dijet asymmetry A_J for 0%–30% centrality, inside ($\Delta R < 0.8$) one of the leading or subleading jet cones (left-hand side) and outside ($\Delta R > 0.8$) the leading and subleading jet cones (right-hand side). For the solid circles, vertical bars and brackets represent the statistical and systematic uncertainties, respectively. For the individual p_T ranges, the statistical uncertainties are shown as vertical bars.

more than 50% of the balance is carried by tracks with $p_T > 4$ GeV/c, with a negligible contribution from $p_T < 1$ GeV/c.

The PYTHIA + HYDJET results are indicative of semi-hard initial- or final-state radiation as the underlying cause for large A_J events in the MC study. This has been confirmed by further studies which showed that in PYTHIA the momentum balance in the transverse plane for events with large A_J can be restored if a third jet with $p_T > 20$ GeV/c, which is present in more than 90% of these events, is included. This is in contrast to the results for large-A_J PbPb data, which show that a large part of the momentum balance is carried by soft particles ($p_T < 2$ GeV/c) and radiated at large angles to the jet axes ($\Delta R > 0.8$) in the direction of the subleading jet.

IV. SUMMARY

The CMS detector has been used to study jet production in PbPb collisions at $\sqrt{s_{NN}} = 2.76$ TeV. Jets were reconstructed using primarily the calorimeter information in a data sample corresponding to an integrated luminosity of $L_{int} = 6.7$ μb^{-1}. Events having a leading jet with $p_T > 120$ GeV/c and $|\eta| < 2$ were selected. As a function of centrality, dijet events with a subleading jet of $p_T > 50$ GeV/c and $|\eta| < 2$ were found to have an increasing momentum imbalance. Data were compared to PYTHIA dijet simulations for pp collisions at the same energy which were embedded into real heavy ion events. The momentum imbalances observed in the data were significantly larger than those predicted by the simulations. While the relative imbalance between the leading and subleading jets increased with increasing collision centrality, it was found to be largely independent of the leading jet p_T, up to the highest p_T region studied ($\approx$210 GeV/c).

The angular distribution of jet fragmentation products has been explored by associating charged tracks with the dijets observed in the calorimeters. The calorimeter-based momentum imbalance is reflected in the associated track distributions, which show a softening and widening of the subleading jet fragmentation pattern for increasing dijet asymmetry, while the high-p_T components of the leading jet remain nearly unchanged.

Studies of the missing transverse momentum projected on the jet axis have shown that the overall momentum balance can be recovered if tracks at low p_T are included. In the PbPb data, but not in the simulations, a large fraction of the balancing momentum is carried by tracks having $p_T < 2$ GeV/c. Comparing the momentum balance inside and outside of cones of $\Delta R = 0.8$ around the leading and subleading jet axes demonstrates that a large contribution to the momentum balance in data arises from soft particles radiated at $\Delta R > 0.8$ to the jets, a feature which is also not reproduced in PYTHIA calculations.

In conclusion, a strong increase in the fraction of highly unbalanced jets has been seen in central PbPb collisions compared with peripheral collisions and model calculations, consistent with a high degree of jet quenching in the produced matter. A large fraction of the momentum balance of these unbalanced jets is carried by low-p_T particles at large radial distance, in contrast to PYTHIA simulations embedded into heavy-ion events. The results provide qualitative constraints on the nature of the jet modification in PbPb collisions and quantitative input to models of the transport properties of the medium created in these collisions.

[1] E. V. Shuryak, Sov. Phys. JETP **47**, 212 (1978) [Zh. Eksp. Teor. Fiz. **74** 408, 1978].

[2] J. C. Collins and M. J. Perry, Phys. Rev. Lett. **34**, 1353 (1975).

[3] N. Cabibbo and G. Parisi, Phys. Lett. B **59**, 67 (1975).

[4] B. A. Freedman and L. D. McLerran, Phys. Rev. D **16**, 1169 (1977).

[5] F. Karsch and E. Laermann, *Quark-Gluon Plasma 3*, edited by R. C. Hwa and X. N. Wang (World Scientific Pub. Co. Inc, Hackensack, NJ, 2004), pp. 1–59.

[6] J. D. Bjorken, Fermilab Report No. FERMILAB-PUB-82-059-THY, 1982 [http://lss.fnal.gov/cgi-bin/find_paper.pl?pub-82-059-T].

[7] J. Casalderrey-Solana and C. A. Salgado, Acta Phys. Pol. B **38**, 3731 (2007).

[8] D. d'Enterria, in *Selective Tracer Signals of the QCD Plasma State*, edited by R. Block, Landolt-Börnstein, New Series, Group I, Vol. 23, Pt. A (Springer, Berlin, 2010), p. 99.

[9] K. Adcox *et al.* (PHENIX Collaboration), Nucl. Phys. A **757**, 184 (2005).

[10] J. Adams *et al.* (STAR Collaboration), Nucl. Phys. A **757**, 102 (2005).

[11] B. B. Back *et al.* (PHOBOS Collaboration), Nucl. Phys. A **757**, 28 (2005).

[12] I. Arsene *et al.* (BRAHMS Collaboration), Nucl. Phys. A **757**, 1 (2005).

[13] S. Salur (STAR Collaboration), Eur. Phys. J. C **61**, 761 (2009).

[14] J. Putschke (STAR Collaboration), Eur. Phys. J. C **61**, 629 (2009).

[15] E. Bruna (STAR Collaboration), Nucl. Phys. A **830**, 267C (2009).

[16] M. Ploskon (STAR Collaboration), Nucl. Phys. A **830**, 255C (2009).

[17] D. A. Appel, Phys. Rev. D **33**, 717 (1986).

[18] J. P. Blaizot and L. D. McLerran, Phys. Rev. D **34**, 2739 (1986).

[19] R. Baier, Y. L. Dokshitzer, A. H. Mueller, S. Peigne, and D. Schiff, Nucl. Phys. B **483**, 291 (1997).

[20] R. Baier, Y. L. Dokshitzer, A. H. Mueller, S. Peigne, and D. Schiff, Nucl. Phys. B **484**, 265 (1997).

[21] R. Baier, Y. L. Dokshitzer, A. H. Mueller, and D. Schiff, Phys. Rev. C **58**, 1706 (1998).

[22] M. Gyulassy, P. Levai, and I. Vitev, Nucl. Phys. B **594**, 371 (2001).

[23] B. G. Zakharov, JETP Lett. **63**, 952 (1996).

[24] U. A. Wiedemann, Nucl. Phys. B **588**, 303 (2000).

[25] C. A. Salgado and U. A. Wiedemann, Phys. Rev. Lett. **93**, 042301 (2004).

[26] C. A. Salgado, Mod. Phys. Lett. A **19**, 271 (2004).

[27] E. Wang and X.-N. Wang, Phys. Rev. Lett. **89**, 162301 (2002).

[28] (ATLAS Collaboration), Phys. Rev. Lett. **105**, 252303 (2010).

[29] CMS Collaboration, JINST **3**, S08004 (2008).

[30] S. Agostinelli *et al.* (GEANT4 Collaboration), Nucl. Instrum. Methods A **506**, 250 (2003).

[31] O. Djuvsland and J. Nystrand, Phys. Rev. C **83**, 041901 (2011).

[32] CMS Collaboration (CMS), Phys. Rev. Lett. **105**, 022002 (2010).

[33] CMS Collaboration, CMS Note, CMS-NOTE-2010-012, 2010 [http://cdsweb.cern.ch/record/1278160?ln=en].

[34] CMS Collaboration, JINST **5**, T03014 (2010).

[35] M. L. Miller, K. Reygers, S. J. Sanders, and P. Steinberg, Annu. Rev. Nucl. Part. Sci. **57**, 205 (2007).

[36] Z.-W. Lin, C. M. Ko, B.-A. Li, B. Zhang, and S. Pal, Phys. Rev. C **72**, 064901 (2005).

[37] H. De Vries, C. W. De Jager, and C. De Vries, At. Data Nucl. Data Tables **36**, 495 (1987).

[38] K. Nakamura *et al.* (Particle Data Group), J. Phys. G **37**, 075021 (2010).

[39] O. Kodolova, I. Vardanian, A. Nikitenko, and A. Oulianov, Eur. Phys. J. C **50**, 117 (2007).

[40] CMS Collaboration, J. Phys. G **34**, 995 (2007).

[41] CMS Collaboration, Report No. CERN-LHCC-2006-001, 2006 [http://cdsweb.cern.ch/record/922757].

[42] J. E. Huth *et al.*, in *Directions for the Decade: Proceedings of the 1990 Summer Study on High Energy Physics : June 25-July 13, 1990, Snowmass, Colorado* (World Scientific Publishing Company, Hackensack, NJ, 1992), pp. 134–136.

[43] CMS Collaboration, (CMS) CMS Physics Analysis Summary No. CMS-PAS-JME-10-010, 2010 (unpublished).

[44] M. Cacciari, G. P. Salam, and G. Soyez, J. High Energy Phys. 04 (2008) 063.

[45] M. Cacciari, G. P. Salam, and G. Soyez, J. High Energy Phys. 04 (2008) 005.

[46] M. Cacciari and G. P. Salam, Phys. Lett. B **659**, 119 (2008).

[47] M. Cacciari, J. Rojo, G. P. Salam, and G. Soyez, Eur. Phys. J. C **71**, 1539 (2011).

[48] CMS Collaboration, CMS Physics Analysis Summary No. CMS-PAS-PFT-09-001, 2009 [http://cdsweb.cern.ch/record/1194487].

[49] CMS Collaboration, CMS Physics Analysis Summary No. CMS-PAS-PFT-10-002, 2010 [http://cdsweb.cern.ch/record/1279341].

[50] T. Sjöstrand, S. Mrenna, and P. Skands, J. High Energy Phys. 05 (2006) 026 (tune D6T with PDFs CTEQ6L1 used for 2.76 TeV, tune Z2 for pp 7 TeV).

[51] I. P. Lokhtin and A. M. Snigirev, Eur. Phys. J. C **45**, 211 (2006).

[52] M. Cacciari, G. P. Salam, and G. Soyez, Eur. Phys. J. C **71**, 1692 (2011).

[53] CMS Collaboration, J. Phys. G **34**, 995 (2007).

[54] CMS Collaboration, CMS Physics Analysis Summary No. CMS-PAS-JME-10-003, 2010 [http://cdsweb.cern.ch/record/1279362].

[55] V. Khachatryan *et al.* (CMS Collaboration), Phys. Rev. Lett. **106**, 122003 (2011).

[56] CMS Collaboration, CMS Physics Analysis Summary, CMS-PAS-JME-10-014, 2011 [http://cdsweb.cern.ch/record/1339945].

S. Chatrchyan,[1] V. Khachatryan,[1] A. M. Sirunyan,[1] A. Tumasyan,[1] W. Adam,[2] T. Bergauer,[2] M. Dragicevic,[2] J. Erö,[2] C. Fabjan,[2] M. Friedl,[2] R. Frühwirth,[2] V. M. Ghete,[2] J. Hammer,[2,a] S. Hänsel,[2] C. Hartl,[2] M. Hoch,[2] N. Hörmann,[2] J. Hrubec,[2] M. Jeitler,[2] G. Kasieczka,[2] W. Kiesenhofer,[2] M. Krammer,[2] D. Liko,[2] I. Mikulec,[2] M. Pernicka,[2] H. Rohringer,[2] R. Schöfbeck,[2] J. Strauss,[2] F. Teischinger,[2] P. Wagner,[2] W. Waltenberger,[2] G. Walzel,[2] E. Widl,[2] C.-E. Wulz,[2] V. Mossolov,[3] N. Shumeiko,[3] J. Suarez Gonzalez,[3] L. Benucci,[4] E. A. De Wolf,[4] X. Janssen,[4] T. Maes,[4] L. Mucibello,[4] S. Ochesanu,[4] B. Roland,[4] R. Rougny,[4] M. Selvaggi,[4] H. Van Haevermaet,[4] P. Van Mechelen,[4] N. Van Remortel,[4] S. Beauceron,[5] F. Blekman,[5] S. Blyweert,[5] J. D'Hondt,[5] O. Devroede,[5] R. Gonzalez Suarez,[5] A. Kalogeropoulos,[5] J. Maes,[5] M. Maes,[5] W. Van Doninck,[5] P. Van Mulders,[5] G. P. Van Onsem,[5] I. Villella,[5] O. Charaf,[6] B. Clerbaux,[6] G. De Lentdecker,[6] V. Dero,[6] A. P. R. Gay,[6] G. H. Hammad,[6] T. Hreus,[6] P. E. Marage,[6] L. Thomas,[6] C. Vander Velde,[6] P. Vanlaer,[6] J. Wickens,[6] V. Adler,[7] S. Costantini,[7] M. Grunewald,[7] B. Klein,[7] A. Marinov,[7] J. Mccartin,[7] D. Ryckbosch,[7] F. Thyssen,[7] M. Tytgat,[7] L. Vanelderen,[7] P. Verwilligen,[7] S. Walsh,[7] N. Zaganidis,[7] S. Basegmez,[8] G. Bruno,[8] J. Caudron,[8] L. Ceard,[8] E. Cortina Gil,[8] C. Delaere,[8] D. Favart,[8] A. Giammanco,[8] G. Grégoire,[8] J. Hollar,[8] V. Lemaitre,[8] J. Liao,[8] O. Militaru,[8] S. Ovyn,[8] D. Pagano,[8] A. Pin,[8] K. Piotrzkowski,[8] N. Schul,[8] N. Beliy,[9] T. Caebergs,[9] E. Daubie,[9] G. A. Alves,[10] D. De Jesus Damiao,[10] M. E. Pol,[10] M. H. G. Souza,[10] W. Carvalho,[11] E. M. Da Costa,[11] C. De Oliveira Martins,[11] S. Fonseca De Souza,[11] L. Mundim,[11] H. Nogima,[11] V. Oguri,[11] W. L. Prado Da Silva,[11] A. Santoro,[11] S. M. Silva Do Amaral,[11] A. Sznajder,[11] F. Torres Da Silva De Araujo,[11] F. A. Dias,[12] T. R. Fernandez Perez Tomei,[12] E. M. Gregores,[12,b] F. Marinho,[12] P. G. Mercadante,[12,b] S. F. Novaes,[12] Sandra S. Padula,[12] N. Darmenov,[13,a] L. Dimitrov,[13] V. Genchev,[13,a] P. Iaydjiev,[13,a] S. Piperov,[13] M. Rodozov,[13] S. Stoykova,[13] G. Sultanov,[13] V. Tcholakov,[13] R. Trayanov,[13] I. Vankov,[13] M. Dyulendarova,[14] R. Hadjiiska,[14] V. Kozhuharov,[14] L. Litov,[14] E. Marinova,[14] M. Mateev,[14] B. Pavlov,[14] P. Petkov,[14] J. G. Bian,[15] G. M. Chen,[15] H. S. Chen,[15] C. H. Jiang,[15] D. Liang,[15] S. Liang,[15] X. Meng,[15] J. Tao,[15] J. Wang,[15] J. Wang,[15] X. Wang,[15] Z. Wang,[15] M. Xu,[15] J. Zang,[15] Z. Zhang,[15] Y. Ban,[16] S. Guo,[16] Y. Guo,[16] W. Li,[16] Y. Mao,[16] S. J. Qian,[16] H. Teng,[16] L. Zhang,[16] B. Zhu,[16] W. Zou,[16] A. Cabrera,[17] B. Gomez Moreno,[17] A. A. Ocampo Rios,[17] A. F. Osorio Oliveros,[17] J. C. Sanabria,[17] N. Godinovic,[18] D. Lelas,[18] K. Lelas,[18] R. Plestina,[18,c] D. Polic,[18] I. Puljak,[18] Z. Antunovic,[19] M. Dzelalija,[19] V. Brigljevic,[20] S. Duric,[20] K. Kadija,[20] S. Morovic,[20] A. Attikis,[21] M. Galanti,[21] J. Mousa,[21] C. Nicolaou,[21] F. Ptochos,[21] P. A. Razis,[21] M. Finger,[22] M. Finger Jr.,[22] Y. Assran,[23,d] S. Khalil,[23,e] M. A. Mahmoud,[23,f] A. Hektor,[24] M. Kadastik,[24] M. Müntel,[24] M. Raidal,[24] L. Rebane,[24] V. Azzolini,[25] P. Eerola,[25] S. Czellar,[26] J. Härkönen,[26] V. Karimäki,[26] R. Kinnunen,[26] M. J. Kortelainen,[26] T. Lampén,[26] K. Lassila-Perini,[26] S. Lehti,[26] T. Lindén,[26] P. Luukka,[26] T. Mäenpää,[26] E. Tuominen,[26] J. Tuominiemi,[26] E. Tuovinen,[26] D. Ungaro,[26] L. Wendland,[26] K. Banzuzi,[27] A. Korpela,[27] T. Tuuva,[27] D. Sillou,[28] M. Besancon,[29] S. Choudhury,[29] M. Dejardin,[29] D. Denegri,[29] B. Fabbro,[29] J. L. Faure,[29] F. Ferri,[29] S. Ganjour,[29] F. X. Gentit,[29] A. Givernaud,[29] P. Gras,[29] G. Hamel de Monchenault,[29] P. Jarry,[29] E. Locci,[29] J. Malcles,[29] M. Marionneau,[29] L. Millischer,[29] J. Rander,[29] A. Rosowsky,[29] I. Shreyber,[29] M. Titov,[29] P. Verrecchia,[29] S. Baffioni,[30] F. Beaudette,[30] L. Benhabib,[30] L. Bianchini,[30] M. Bluj,[30,g] C. Broutin,[30] P. Busson,[30] C. Charlot,[30] T. Dahms,[30] L. Dobrzynski,[30] S. Elgammal,[30] R. Granier de Cassagnac,[30] M. Haguenauer,[30] P. Miné,[30] C. Mironov,[30] C. Ochando,[30] P. Paganini,[30] T. Roxlo,[30] D. Sabes,[30] R. Salerno,[30] Y. Sirois,[30] C. Thiebaux,[30] B. Wyslouch,[30,h] A. Zabi,[30] J.-L. Agram,[31,i] J. Andrea,[31] D. Bloch,[31] D. Bodin,[31] J.-M. Brom,[31] M. Cardaci,[31] E. C. Chabert,[31] C. Collard,[31] E. Conte,[31,i] F. Drouhin,[31,i] C. Ferro,[31] J.-C. Fontaine,[31,i] D. Gelé,[31] U. Goerlach,[31] S. Greder,[31] P. Juillot,[31] M. Karim,[31,i] A.-C. Le Bihan,[31] Y. Mikami,[31] P. Van Hove,[31] F. Fassi,[32] D. Mercier,[32] C. Baty,[33] N. Beaupere,[33] M. Bedjidian,[33] O. Bondu,[33] G. Boudoul,[33] D. Boumediene,[33] H. Brun,[33] N. Chanon,[33] R. Chierici,[33] D. Contardo,[33] P. Depasse,[33] H. El Mamouni,[33] A. Falkiewicz,[33] J. Fay,[33] S. Gascon,[33] B. Ille,[33] T. Kurca,[33] T. Le Grand,[33] M. Lethuillier,[33] L. Mirabito,[33] S. Perries,[33] V. Sordini,[33] S. Tosi,[33] Y. Tschudi,[33] P. Verdier,[33] H. Xiao,[33] L. Megrelidze,[34] D. Lomidze,[35] G. Anagnostou,[36] M. Edelhoff,[36] L. Feld,[36] N. Heracleous,[36] O. Hindrichs,[36] R. Jussen,[36] K. Klein,[36] J. Merz,[36] N. Mohr,[36] A. Ostapchuk,[36] A. Perieanu,[36] F. Raupach,[36] J. Sammet,[36] S. Schael,[36] D. Sprenger,[36] H. Weber,[36] M. Weber,[36] B. Wittmer,[36] M. Ata,[37] W. Bender,[37] M. Erdmann,[37] J. Frangenheim,[37] T. Hebbeker,[37] A. Hinzmann,[37] K. Hoepfner,[37] C. Hof,[37] T. Klimkovich,[37] D. Klingebiel,[37] P. Kreuzer,[37] D. Lanske,[37,j] C. Magass,[37] G. Masetti,[37] M. Merschmeyer,[37] A. Meyer,[37] P. Papacz,[37] H. Pieta,[37] H. Reithler,[37] S. A. Schmitz,[37] L. Sonnenschein,[37] J. Steggemann,[37] D. Teyssier,[37] M. Tonutti,[37] M. Bontenackels,[38] M. Davids,[38] M. Duda,[38] G. Flügge,[38] H. Geenen,[38] M. Giffels,[38] W. Haj Ahmad,[38] D. Heydhausen,[38] T. Kress,[38] Y. Kuessel,[38] A. Linn,[38] A. Nowack,[38] L. Perchalla,[38] O. Pooth,[38] J. Rennefeld,[38] P. Sauerland,[38] A. Stahl,[38] M. Thomas,[38] D. Tornier,[38] M. H. Zoeller,[38] M. Aldaya Martin,[39] W. Behrenhoff,[39] U. Behrens,[39] M. Bergholz,[39,k] K. Borras,[39] A. Cakir,[39] A. Campbell,[39] E. Castro,[39] D. Dammann,[39] G. Eckerlin,[39] D. Eckstein,[39] A. Flossdorf,[39] G. Flucke,[39] A. Geiser,[39] J. Hauk,[39] H. Jung,[39] M. Kasemann,[39] I. Katkov,[39] P. Katsas,[39] C. Kleinwort,[39] H. Kluge,[39] A. Knutsson,[39] M. Krämer,[39] D. Krücker,[39] E. Kuznetsova,[39] W. Lange,[39] W. Lohmann,[39,k] R. Mankel,[39] M. Marienfeld,[39] I.-A. Melzer-Pellmann,[39] A. B. Meyer,[39] J. Mnich,[39] A. Mussgiller,[39] J. Olzem,[39] D. Pitzl,[39] A. Raspereza,[39] A. Raval,[39] M. Rosin,[39] R. Schmidt,[39,k] T. Schoerner-Sadenius,[39] N. Sen,[39] A. Spiridonov,[39] M. Stein,[39] J. Tomaszewska,[39] R. Walsh,[39] C. Wissing,[39] C. Autermann,[40] S. Bobrovskyi,[40] J. Draeger,[40] H. Enderle,[40] U. Gebbert,[40] K. Kaschube,[40] G. Kaussen,[40] J. Lange,[40] B. Mura,[40] S. Naumann-Emme,[40] F. Nowak,[40] N. Pietsch,[40] C. Sander,[40] H. Schettler,[40] P. Schleper,[40] M. Schröder,[40] T. Schum,[40] J. Schwandt,[40] H. Stadie,[40] G. Steinbrück,[40] J. Thomsen,[40] C. Barth,[41] J. Bauer,[41] V. Buege,[41] T. Chwalek,[41] W. De Boer,[41] A. Dierlamm,[41] G. Dirkes,[41] M. Feindt,[41] J. Gruschke,[41] C. Hackstein,[41] F. Hartmann,[41] S. M. Heindl,[41] M. Heinrich,[41] H. Held,[41] K. H. Hoffmann,[41] S. Honc,[41] T. Kuhr,[41] D. Martschei,[41] S. Mueller,[41] Th. Müller,[41] M. Niegel,[41] O. Oberst,[41] A. Oehler,[41] J. Ott,[41] T. Peiffer,[41] D. Piparo,[41]

G. Quast,[41] K. Rabbertz,[41] F. Ratnikov,[41] N. Ratnikova,[41] M. Renz,[41] C. Saout,[41] A. Scheurer,[41] P. Schieferdecker,[41] F.-P. Schilling,[41] M. Schmanau,[41] G. Schott,[41] H. J. Simonis,[41] F. M. Stober,[41] D. Troendle,[41] J. Wagner-Kuhr,[41] T. Weiler,[41] M. Zeise,[41] V. Zhukov,[41,l] E. B. Ziebarth,[41] G. Daskalakis,[42] T. Geralis,[42] K. Karafasoulis,[42] S. Kesisoglou,[42] A. Kyriakis,[42] D. Loukas,[42] I. Manolakos,[42] A. Markou,[42] C. Markou,[42] C. Mavrommatis,[42] E. Ntomari,[42] E. Petrakou,[42] L. Gouskos,[43] T. J. Mertzimekis,[43] A. Panagiotou,[43] I. Evangelou,[44] C. Foudas,[44] P. Kokkas,[44] N. Manthos,[44] I. Papadopoulos,[44] V. Patras,[44] F. A. Triantis,[44] G. Aranyi,[45] G. Bencze,[45] L. Boldizsar,[45] C. Hajdu,[45,a] P. Hidas,[45] D. Horvath,[45,m] A. Kapusi,[45] K. Krajczar,[45,n] F. Sikler,[45] G. I. Veres,[45,n] G. Vesztergombi,[45,n] N. Beni,[46] J. Molnar,[46] J. Palinkas,[46] Z. Szillasi,[46] V. Veszpremi,[46] P. Raics,[47] Z. L. Trocsanyi,[47] B. Ujvari,[47] S. Bansal,[48] S. B. Beri,[48] V. Bhatnagar,[48] N. Dhingra,[48] R. Gupta,[48] M. Jindal,[48] M. Kaur,[48] J. M. Kohli,[48] M. Z. Mehta,[48] N. Nishu,[48] L. K. Saini,[48] A. Sharma,[48] A. P. Singh,[48] J. B. Singh,[48] S. P. Singh,[48] S. Ahuja,[49] S. Bhattacharya,[49] B.C. Choudhary,[49] P. Gupta,[49] S. Jain,[49] S. Jain,[49] A. Kumar,[49] K. Ranjan,[49] R. K. Shivpuri,[49] R. K. Choudhury,[50] D. Dutta,[50] S. Kailas,[50] A. K. Mohanty,[50,a] L. M. Pant,[50] P. Shukla,[50] T. Aziz,[51] M. Guchait,[51,o] A. Gurtu,[51] M. Maity,[51,p] D. Majumder,[51] G. Majumder,[51] K. Mazumdar,[51] G. B. Mohanty,[51] A. Saha,[51] K. Sudhakar,[51] N. Wickramage,[51] S. Banerjee,[52] S. Dugad,[52] N. K. Mondal,[52] H. Arfaei,[53] H. Bakhshiansohi,[53] S. M. Etesami,[53] A. Fahim,[53] M. Hashemi,[53] A. Jafari,[53] M. Khakzad,[53] A. Mohammadi,[53] M. Mohammadi Najafabadi,[53] S. Paktinat Mehdiabadi,[53] B. Safarzadeh,[53] M. Zeinali,[53] M. Abbrescia,[54a,54b] L. Barbone,[54a,54b] C. Calabria,[54a,54b] A. Colaleo,[54a] D. Creanza,[54a,54c] N. De Filippis,[54a,54c] M. De Palma,[54a,54b] A. Dimitrov,[54a] L. Fiore,[54a] G. Iaselli,[54a,54c] L. Lusito,[54a,54b,a] G. Maggi,[54a,54c] M. Maggi,[54a] N. Manna,[54a,54b] B. Marangelli,[54a,54b] S. My,[54a,54c] S. Nuzzo,[54a,54b] N. Pacifico,[54a,54b] G. A. Pierro,[54a] A. Pompili,[54a,54b] G. Pugliese,[54a,54c] F. Romano,[54a,54c] G. Roselli,[54a,54b] G. Selvaggi,[54a,54b] L. Silvestris,[54a] R. Trentadue,[54a] S. Tupputi,[54a,54b] G. Zito,[54a] G. Abbiendi,[55a] A. C. Benvenuti,[55a] D. Bonacorsi,[55a] S. Braibant-Giacomelli,[55a,55b] L. Brigliadori,[55a] P. Capiluppi,[55a,55b] A. Castro,[55a,55b] F. R. Cavallo,[55a] M. Cuffiani,[55a,55b] G. M. Dallavalle,[55a] F. Fabbri,[55a] A. Fanfani,[55a,55b] D. Fasanella,[55a] P. Giacomelli,[55a] M. Giunta,[55a] S. Marcellini,[55a] M. Meneghelli,[55a,55b] A. Montanari,[55a] F. L. Navarria,[55a,55b] F. Odorici,[55a] A. Perrotta,[55a] F. Primavera,[55a] A. M. Rossi,[55a,55b] T. Rovelli,[55a,55b] G. Siroli,[55a,55b] R. Travaglini,[55a,55b] S. Albergo,[56a,56b] G. Cappello,[56a,56b] M. Chiorboli,[56a,56b,a] S. Costa,[56a,56b] A. Tricomi,[56a,56b] C. Tuve,[56a] G. Barbagli,[57a] V. Ciulli,[57a,57b] C. Civinini,[57a] R. D'Alessandro,[57a,57b] E. Focardi,[57a,57b] S. Frosali,[57a,57b] E. Gallo,[57a] S. Gonzi,[57a,57b] P. Lenzi,[57a,57b] M. Meschini,[57a] S. Paoletti,[57a] G. Sguazzoni,[57a] A. Tropiano,[57a,a] L. Benussi,[58] S. Bianco,[58] S. Colafranceschi,[58,q] F. Fabbri,[58] D. Piccolo,[58] P. Fabbricatore,[59] R. Musenich,[59] A. Benaglia,[60a,60b] F. De Guio,[60a,60b,a] L. Di Matteo,[60a,60b] A. Ghezzi,[60a,60b,a] M. Malberti,[60a,60b] S. Malvezzi,[60a] A. Martelli,[60a,60b] A. Massironi,[60a,60b] D. Menasce,[60a] L. Moroni,[60a] M. Paganoni,[60a,60b] D. Pedrini,[60a] S. Ragazzi,[60a,60b] N. Redaelli,[60a] S. Sala,[60a] T. Tabarelli de Fatis,[60a,60b] V. Tancini,[60a,60b] S. Buontempo,[61a] C. A. Carrillo Montoya,[61a] N. Cavallo,[61a,r] A. Cimmino,[61a,61b] A. De Cosa,[61a,61b] M. De Gruttola,[61a,61b] F. Fabozzi,[61a,r] A. O. M. Iorio,[61a] L. Lista,[61a] M. Merola,[61a,61b] P. Noli,[61a,61b] P. Paolucci,[61a] P. Azzi,[62a] N. Bacchetta,[62a] P. Bellan,[62a,62b] D. Bisello,[62a,62b] A. Branca,[62a] R. Carlin,[62a,62b] P. Checchia,[62a] M. De Mattia,[62a,62b] T. Dorigo,[62a] U. Dosselli,[62a] F. Fanzago,[62a] F. Gasparini,[62a,62b] U. Gasparini,[62a,62b] S. Lacaprara,[62a,s] I. Lazzizzera,[62a,62c] M. Margoni,[62a,62b] M. Mazzucato,[62a] A. T. Meneguzzo,[62a,62b] M. Nespolo,[62a] L. Perrozzi,[62a,a] N. Pozzobon,[62a,62b] P. Ronchese,[62a,62b] F. Simonetto,[62a,62b] E. Torassa,[62a] M. Tosi,[62a,62b] S. Vanini,[62a,62b] P. Zotto,[62a,62b] G. Zumerle,[62a,62b] U. Berzano,[63a] S. P. Ratti,[63a,63b] C. Riccardi,[63a,63b] P. Vitulo,[63a,63b] M. Biasini,[64a,64b] G. M. Bilei,[64a] B. Caponeri,[64a,64b] L. Fanò,[64a,64b] P. Lariccia,[64a,64b] A. Lucaroni,[64a,64b,a] G. Mantovani,[64a,64b] M. Menichelli,[64a] A. Nappi,[64a,64b] A. Santocchia,[64a,64b] S. Taroni,[64a,64b] M. Valdata,[64a,64b] R. Volpe,[64a,64b,a] P. Azzurri,[65a,65c] G. Bagliesi,[65a] J. Bernardini,[65a,65b] T. Boccali,[65a,a] G. Broccolo,[65a,65c] R. Castaldi,[65a] R. T. D'Agnolo,[65a,65c] R. Dell'Orso,[65a] F. Fiori,[65a,65b] L. Foà,[65a,65c] A. Giassi,[65a] A. Kraan,[65a] F. Ligabue,[65a,65c] T. Lomtadze,[65a] L. Martini,[65a,t] A. Messineo,[65a,65b] F. Palla,[65a] F. Palmonari,[65a] G. Segneri,[65a] A. T. Serban,[65a] P. Spagnolo,[65a] R. Tenchini,[65a] G. Tonelli,[65a,65b,a] A. Venturi,[65a,a] P. G. Verdini,[65a] L. Barone,[66a,66b] F. Cavallari,[66a] D. Del Re,[66a,66b] E. Di Marco,[66a,66b] M. Diemoz,[66a] D. Franci,[66a,66b] M. Grassi,[66a] E. Longo,[66a,66b] S. Nourbakhsh,[66a] G. Organtini,[66a,66b] A. Palma,[66a,66b] F. Pandolfi,[66a,66b,a] R. Paramatti,[66a] S. Rahatlou,[66a,66b] N. Amapane,[67a,67b] R. Arcidiacono,[67a,67c] S. Argiro,[67a,67b] M. Arneodo,[67a,67c] C. Biino,[67a] C. Botta,[67a,67b,a] N. Cartiglia,[67a] R. Castello,[67a,67b] M. Costa,[67a,67b] N. Demaria,[67a] A. Graziano,[67a,67b,a] C. Mariotti,[67a] M. Marone,[67a,67b] S. Maselli,[67a] E. Migliore,[67a,67b] G. Mila,[67a,67b] V. Monaco,[67a,67b] M. Musich,[67a] M. M. Obertino,[67a,67c] N. Pastrone,[67a] M. Pelliccioni,[67a,67b,a] A. Romero,[67a,67b] M. Ruspa,[67a,67c] R. Sacchi,[67a,67b] V. Sola,[67a,67b] A. Solano,[67a,67b] A. Staiano,[67a] D. Trocino,[67a,67b] A. Vilela Pereira,[67a,67b,a] S. Belforte,[68a] F. Cossutti,[68a] G. Della Ricca,[68a,68b] B. Gobbo,[68a] D. Montanino,[68a,68b] A. Penzo,[68a] S. G. Heo,[69] S. K. Nam,[69] S. Chang,[70] J. Chung,[70] D. H. Kim,[70] G. N. Kim,[70] J. E. Kim,[70] D. J. Kong,[70] H. Park,[70] S. R. Ro,[70] D. Son,[70] D. C. Son,[70] Zero Kim,[71] J. Y. Kim,[71] S. Song,[71] S. Choi,[72] B. Hong,[72] M. Jo,[72] H. Kim,[72] J. H. Kim,[72] T. J. Kim,[72] K. S. Lee,[72] D. H. Moon,[72] S. K. Park,[72] H. B. Rhee,[72] E. Seo,[72] S. Shin,[72] K. S. Sim,[72] M. Choi,[73] S. Kang,[73] H. Kim,[73] C. Park,[73] I. C. Park,[73] S. Park,[73] G. Ryu,[73] Y. Choi,[74] Y. K. Choi,[74] J. Goh,[74] M. S. Kim,[74] J. Lee,[74] S. Lee,[74] H. Seo,[74] I. Yu,[74] M. J. Bilinskas,[75] I. Grigelionis,[75] M. Janulis,[75] D. Martisiute,[75] P. Petrov,[75] T. Sabonis,[75] H. Castilla-Valdez,[76] E. De La Cruz-Burelo,[76] R. Lopez-Fernandez,[76] A. Sánchez-Hernández,[76] L. M. Villasenor-Cendejas,[76] S. Carrillo Moreno,[77] F. Vazquez Valencia,[77] H. A. Salazar Ibarguen,[78] E. Casimiro Linares,[79] A. Morelos Pineda,[79] M. A. Reyes-Santos,[79] D. Krofcheck,[80] P. H. Butler,[81] R. Doesburg,[81] H. Silverwood,[81] M. Ahmad,[82] I. Ahmed,[82] M. I. Asghar,[82] H. R. Hoorani,[82] W. A. Khan,[82] T. Khurshid,[82] S. Qazi,[82] M. Cwiok,[83] W. Dominik,[83] K. Doroba,[83] A. Kalinowski,[83] M. Konecki,[83] J. Krolikowski,[83] T. Frueboes,[84] R. Gokieli,[84] M. Górski,[84] M. Kazana,[84] K. Nawrocki,[84] K. Romanowska-Rybinska,[84] M. Szleper,[84] G. Wrochna,[84] P. Zalewski,[84] N. Almeida,[85] P. Bargassa,[85] A. David,[85] P. Faccioli,[85] P. G. Ferreira Parracho,[85]

M. Gallinaro,[85] P. Musella,[85] A. Nayak,[85] J. Seixas,[85] J. Varela,[85] S. Afanasiev,[86] I. Belotelov,[86] P. Bunin,[86] I. Golutvin,[86] A. Kamenev,[86] V. Karjavin,[86] G. Kozlov,[86] A. Lanev,[86] P. Moisenz,[86] V. Palichik,[86] V. Perelygin,[86] S. Shmatov,[86] V. Smirnov,[86] A. Volodko,[86] A. Zarubin,[86] V. Golovtsov,[87] Y. Ivanov,[87] V. Kim,[87] P. Levchenko,[87] V. Murzin,[87] V. Oreshkin,[87] I. Smirnov,[87] V. Sulimov,[87] L. Uvarov,[87] S. Vavilov,[87] A. Vorobyev,[87] A. Vorobyev,[87] Yu. Andreev,[88] A. Dermenev,[88] S. Gninenko,[88] N. Golubev,[88] M. Kirsanov,[88] N. Krasnikov,[88] N. Matveev,[88] A. Pashenkov,[88] A. Toropin,[88] S. Troitsky,[88] V. Epshteyn,[89] V. Gavrilov,[89] V. Kaftanov,[89,j] M. Kossov,[89,a] A. Krokhotin,[89] N. Lychkovskaya,[89] V. Popov,[89] G. Safronov,[89] S. Semenov,[89] V. Stolin,[89] E. Vlasov,[89] A. Zhokin,[89] A. Ershov,[90] A. Gribushin,[90] O. Kodolova,[90] V. Korotkikh,[90] I. Lokhtin,[90] S. Obraztsov,[90] S. Petrushanko,[90] A. Proskuryakov,[90] L. Sarycheva,[90] V. Savrin,[90] A. Snigirev,[90] I. Vardanyan,[90] V. Andreev,[91] M. Azarkin,[91] I. Dremin,[91] M. Kirakosyan,[91] A. Leonidov,[91] S. V. Rusakov,[91] A. Vinogradov,[91] I. Azhgirey,[92] S. Bitioukov,[92] V. Grishin,[92,a] V. Kachanov,[92] D. Konstantinov,[92] A. Korablev,[92] V. Krychkine,[92] V. Petrov,[92] R. Ryutin,[92] S. Slabospitsky,[92] A. Sobol,[92] L. Tourtchanovitch,[92] S. Troshin,[92] N. Tyurin,[92] A. Uzunian,[92] A. Volkov,[92] P. Adzic,[93,u] M. Djordjevic,[93] D. Krpic,[93,u] J. Milosevic,[93] M. Aguilar-Benitez,[94] J. Alcaraz Maestre,[94] P. Arce,[94] C. Battilana,[94] E. Calvo,[94] M. Cepeda,[94] M. Cerrada,[94] N. Colino,[94] B. De La Cruz,[94] A. Delgado Peris,[94] C. Diez Pardos,[94] D. Domínguez Vázquez,[94] C. Fernandez Bedoya,[94] J. P. Fernández Ramos,[94] A. Ferrando,[94] J. Flix,[94] M. C. Fouz,[94] P. Garcia-Abia,[94] O. Gonzalez Lopez,[94] S. Goy Lopez,[94] J. M. Hernandez,[94] M. I. Josa,[94] G. Merino,[94] J. Puerta Pelayo,[94] I. Redondo,[94] L. Romero,[94] J. Santaolalla,[94] C. Willmott,[94] C. Albajar,[95] G. Codispoti,[95] J. F. de Trocóniz,[95] J. Cuevas,[96] J. Fernandez Menendez,[96] S. Folgueras,[96] I. Gonzalez Caballero,[96] L. Lloret Iglesias,[96] J. M. Vizan Garcia,[96] J. A. Brochero Cifuentes,[97] I. J. Cabrillo,[97] A. Calderon,[97] M. Chamizo Llatas,[97] S. H. Chuang,[97] J. Duarte Campderros,[97] M. Felcini,[97,v] M. Fernandez,[97] G. Gomez,[97] J. Gonzalez Sanchez,[97] C. Jorda,[97] P. Lobelle Pardo,[97] A. Lopez Virto,[97] J. Marco,[97] R. Marco,[97] C. Martinez Rivero,[97] F. Matorras,[97] F. J. Munoz Sanchez,[97] J. Piedra Gomez,[97,w] T. Rodrigo,[97] A. Y. Rodríguez-Marrero,[97] A. Ruiz-Jimeno,[97] L. Scodellaro,[97] M. Sobron Sanudo,[97] I. Vila,[97] R. Vilar Cortabitarte,[97] D. Abbaneo,[98] E. Auffray,[98] G. Auzinger,[98] P. Baillon,[98] A. H. Ball,[98] D. Barney,[98] A. J. Bell,[98,x] D. Benedetti,[98] C. Bernet,[98,c] W. Bialas,[98] P. Bloch,[98] A. Bocci,[98] S. Bolognesi,[98] M. Bona,[98] H. Breuker,[98] G. Brona,[98] K. Bunkowski,[98] T. Camporesi,[98] G. Cerminara,[98] J. A. Coarasa Perez,[98] B. Curé,[98] D. D'Enterria,[98] A. De Roeck,[98] S. Di Guida,[98] A. Elliott-Peisert,[98] B. Frisch,[98] W. Funk,[98] A. Gaddi,[98] S. Gennai,[98] G. Georgiou,[98] H. Gerwig,[98] D. Gigi,[98] K. Gill,[98] D. Giordano,[98] F. Glege,[98] R. Gomez-Reino Garrido,[98] M. Gouzevitch,[98] P. Govoni,[98] S. Gowdy,[98] L. Guiducci,[98] M. Hansen,[98] J. Harvey,[98] J. Hegeman,[98] B. Hegner,[98] H. F. Hoffmann,[98] A. Honma,[98] V. Innocente,[98] P. Janot,[98] K. Kaadze,[98] E. Karavakis,[98] P. Lecoq,[98] C. Lourenço,[98] A. Macpherson,[98] T. Mäki,[98] L. Malgeri,[98] M. Mannelli,[98] L. Masetti,[98] F. Meijers,[98] S. Mersi,[98] E. Meschi,[98] R. Moser,[98] M. U. Mozer,[98] M. Mulders,[98] E. Nesvold,[98,a] M. Nguyen,[98] T. Orimoto,[98] L. Orsini,[98] E. Perez,[98] A. Petrilli,[98] A. Pfeiffer,[98] M. Pierini,[98] M. Pimiä,[98] G. Polese,[98] A. Racz,[98] J. Rodrigues Antunes,[98] G. Rolandi,[98,y] T. Rommerskirchen,[98] C. Rovelli,[98,z] M. Rovere,[98] H. Sakulin,[98] C. Schäfer,[98] C. Schwick,[98] I. Segoni,[98] A. Sharma,[98] P. Siegrist,[98] M. Simon,[98] P. Sphicas,[98,aa] M. Spiropulu,[98,bb] F. Stöckli,[98] M. Stoye,[98] P. Tropea,[98] A. Tsirou,[98] P. Vichoudis,[98] M. Voutilainen,[98] W. D. Zeuner,[98] W. Bertl,[99] K. Deiters,[99] W. Erdmann,[99] K. Gabathuler,[99] R. Horisberger,[99] Q. Ingram,[99] H. C. Kaestli,[99] S. König,[99] D. Kotlinski,[99] U. Langenegger,[99] F. Meier,[99] D. Renker,[99] T. Rohe,[99] J. Sibille,[99,cc] A. Starodumov,[99,dd] P. Bortignon,[100] L. Caminada,[100,ee] Z. Chen,[100] S. Cittolin,[100] G. Dissertori,[100] M. Dittmar,[100] J. Eugster,[100] K. Freudenreich,[100] C. Grab,[100] A. Hervé,[100] W. Hintz,[100] P. Lecomte,[100] W. Lustermann,[100] C. Marchica,[100,ee] P. Martinez Ruiz del Arbol,[100] P. Meridiani,[100] P. Milenovic,[100,ff] F. Moortgat,[100] P. Nef,[100] F. Nessi-Tedaldi,[100] L. Pape,[100] F. Pauss,[100] T. Punz,[100] A. Rizzi,[100] F. J. Ronga,[100] M. Rossini,[100] L. Sala,[100] A. K. Sanchez,[100] M.-C. Sawley,[100] B. Stieger,[100] L. Tauscher,[100,j] A. Thea,[100] K. Theofilatos,[100] D. Treille,[100] C. Urscheler,[100] R. Wallny,[100] M. Weber,[100] L. Wehrli,[100] J. Weng,[100] E. Aguiló,[101] C. Amsler,[101] V. Chiochia,[101] S. De Visscher,[101] C. Favaro,[101] M. Ivova Rikova,[101] B. Millan Mejias,[101] C. Regenfus,[101] P. Robmann,[101] A. Schmidt,[101] H. Snoek,[101] Y. H. Chang,[102] E. A. Chen,[102] K. H. Chen,[102] W. T. Chen,[102] S. Dutta,[102] C. M. Kuo,[102] S. W. Li,[102] W. Lin,[102] M. H. Liu,[102] Z. K. Liu,[102] Y. J. Lu,[102] D. Mekterovic,[102] J. H. Wu,[102] S. S. Yu,[102] P. Bartalini,[103] P. Chang,[103] Y. H. Chang,[103] Y. W. Chang,[103] Y. Chao,[103] K. F. Chen,[103] W.-S. Hou,[103] Y. Hsiung,[103] K. Y. Kao,[103] Y. J. Lei,[103] R.-S. Lu,[103] J. G. Shiu,[103] Y. M. Tzeng,[103] M. Wang,[103] A. Adiguzel,[104] Z. Demir,[104] C. Dozen,[104] I. Dumanoglu,[104] E. Eskut,[104] S. Girgis,[104] G. Gokbulut,[104] Y. Guler,[104] E. Gurpinar,[104] I. Hos,[104] E. E. Kangal,[104] T. Karaman,[104] A. Kayis Topaksu,[104] A. Nart,[104] G. Onengut,[104] K. Ozdemir,[104] S. Ozturk,[104] A. Polatoz,[104] K. Sogut,[104,gg] D. Sunar Cerci,[104,hh] D. Uzun,[104] L. N. Vergili,[104] M. Vergili,[104] C. Zorbilmez,[104] I. V. Akin,[105] T. Aliev,[105] S. Bilmis,[105] M. Deniz,[105] H. Gamsizkan,[105] A. M. Guler,[105] K. Ocalan,[105] A. Ozpineci,[105] M. Serin,[105] R. Sever,[105] U. E. Surat,[105] E. Yildirim,[105] M. Zeyrek,[105] M. Deliomeroglu,[106] D. Demir,[106,ii] E. Gülmez,[106] A. Halu,[106] B. Isildak,[106] M. Kaya,[106,jj] O. Kaya,[106,jj] S. Ozkorucuklu,[106,kk] N. Sonmez,[106,ll] L. Levchuk,[107] P. Bell,[108] F. Bostock,[108] J. J. Brooke,[108] T. L. Cheng,[108] E. Clement,[108] D. Cussans,[108] R. Frazier,[108] J. Goldstein,[108] M. Grimes,[108] M. Hansen,[108] D. Hartley,[108] G. P. Heath,[108] H. F. Heath,[108] B. Huckvale,[108] J. Jackson,[108] L. Kreczko,[108] S. Metson,[108] D. M. Newbold,[108,mm] K. Nirunpong,[108] A. Poll,[108] S. Senkin,[108] V. J. Smith,[108] S. Ward,[108] L. Basso,[109,nn] K. W. Bell,[109] A. Belyaev,[109,nn] C. Brew,[109] R. M. Brown,[109] B. Camanzi,[109] D. J. A. Cockerill,[109] J. A. Coughlan,[109] K. Harder,[109] S. Harper,[109] B. W. Kennedy,[109] E. Olaiya,[109] D. Petyt,[109] B. C. Radburn-Smith,[109] C. H. Shepherd-Themistocleous,[109] I. R. Tomalin,[109] W. J. Womersley,[109] S. D. Worm,[109] R. Bainbridge,[110] G. Ball,[110] J. Ballin,[110] R. Beuselinck,[110] O. Buchmuller,[110] D. Colling,[110] N. Cripps,[110] M. Cutajar,[110] G. Davies,[110] M. Della Negra,[110] J. Fulcher,[110] D. Futyan,[110] A. Guneratne Bryer,[110] G. Hall,[110] Z. Hatherell,[110] J. Hays,[110] G. Iles,[110] G. Karapostoli,[110] B. C. MacEvoy,[110] A.-M. Magnan,[110] J. Marrouche,[110] R. Nandi,[110] J. Nash,[110] A. Nikitenko,[110,dd] A. Papageorgiou,[110]

M. Pesaresi,[110] K. Petridis,[110] M. Pioppi,[110,oo] D. M. Raymond,[110] N. Rompotis,[110] A. Rose,[110] M. J. Ryan,[110] C. Seez,[110] P. Sharp,[110] A. Sparrow,[110] A. Tapper,[110] M. Vazquez Acosta,[110] T. Virdee,[110] S. Wakefield,[110] T. Whyntie,[110] M. Barrett,[111] M. Chadwick,[111] J. E. Cole,[111] P. R. Hobson,[111] A. Khan,[111] P. Kyberd,[111] D. Leslie,[111] W. Martin,[111] I. D. Reid,[111] L. Teodorescu,[111] K. Hatakeyama,[112] T. Bose,[113] E. Carrera Jarrin,[113] C. Fantasia,[113] A. Heister,[113] J. St. John,[113] P. Lawson,[113] D. Lazic,[113] J. Rohlf,[113] D. Sperka,[113] L. Sulak,[113] A. Avetisyan,[114] S. Bhattacharya,[114] J. P. Chou,[114] D. Cutts,[114] A. Ferapontov,[114] U. Heintz,[114] S. Jabeen,[114] G. Kukartsev,[114] G. Landsberg,[114] M. Narain,[114] D. Nguyen,[114] M. Segala,[114] T. Speer,[114] K. V. Tsang,[114] R. Breedon,[115] M. Calderon De La Barca Sanchez,[115] S. Chauhan,[115] M. Chertok,[115] J. Conway,[115] P. T. Cox,[115] J. Dolen,[115] R. Erbacher,[115] E. Friis,[115] W. Ko,[115] A. Kopecky,[115] R. Lander,[115] H. Liu,[115] S. Maruyama,[115] T. Miceli,[115] M. Nikolic,[115] D. Pellett,[115] J. Robles,[115] S. Salur,[115] T. Schwarz,[115] M. Searle,[115] J. Smith,[115] M. Squires,[115] M. Tripathi,[115] R. Vasquez Sierra,[115] C. Veelken,[115] V. Andreev,[116] K. Arisaka,[116] D. Cline,[116] R. Cousins,[116] A. Deisher,[116] J. Duris,[116] S. Erhan,[116] C. Farrell,[116] J. Hauser,[116] M. Ignatenko,[116] C. Jarvis,[116] C. Plager,[116] G. Rakness,[116] P. Schlein,[116,j] J. Tucker,[116] V. Valuev,[116] J. Babb,[117] A. Chandra,[117] R. Clare,[117] J. Ellison,[117] J. W. Gary,[117] F. Giordano,[117] G. Hanson,[117] G. Y. Jeng,[117] S. C. Kao,[117] F. Liu,[117] H. Liu,[117] O. R. Long,[117] A. Luthra,[117] H. Nguyen,[117] B. C. Shen,[117,j] R. Stringer,[117] J. Sturdy,[117] S. Sumowidagdo,[117] R. Wilken,[117] S. Wimpenny,[117] W. Andrews,[118] J. G. Branson,[118] G. B. Cerati,[118] E. Dusinberre,[118] D. Evans,[118] F. Golf,[118] A. Holzner,[118] R. Kelley,[118] M. Lebourgeois,[118] J. Letts,[118] B. Mangano,[118] S. Padhi,[118] C. Palmer,[118] G. Petrucciani,[118] H. Pi,[118] M. Pieri,[118] R. Ranieri,[118] M. Sani,[118] V. Sharma,[118,a] S. Simon,[118] Y. Tu,[118] A. Vartak,[118] S. Wasserbaech,[118,pp] F. Würthwein,[118] A. Yagil,[118] D. Barge,[119] R. Bellan,[119] C. Campagnari,[119] M. D'Alfonso,[119] T. Danielson,[119] K. Flowers,[119] P. Geffert,[119] J. Incandela,[119] C. Justus,[119] P. Kalavase,[119] S. A. Koay,[119] D. Kovalskyi,[119] V. Krutelyov,[119] S. Lowette,[119] N. Mccoll,[119] V. Pavlunin,[119] F. Rebassoo,[119] J. Ribnik,[119] J. Richman,[119] R. Rossin,[119] D. Stuart,[119] W. To,[119] J. R. Vlimant,[119] A. Apresyan,[120] A. Bornheim,[120] J. Bunn,[120] Y. Chen,[120] M. Gataullin,[120] Y. Ma,[120] A. Mott,[120] H. B. Newman,[120] C. Rogan,[120] V. Timciuc,[120] P. Traczyk,[120] J. Veverka,[120] R. Wilkinson,[120] Y. Yang,[120] R. Y. Zhu,[120] B. Akgun,[121] R. Carroll,[121] T. Ferguson,[121] Y. Iiyama,[121] D. W. Jang,[121] S. Y. Jun,[121] Y. F. Liu,[121] M. Paulini,[121] J. Russ,[121] H. Vogel,[121] I. Vorobiev,[121] J. P. Cumalat,[122] M. E. Dinardo,[122] B. R. Drell,[122] C. J. Edelmaier,[122] W. T. Ford,[122] A. Gaz,[122] B. Heyburn,[122] E. Luiggi Lopez,[122] U. Nauenberg,[122] J. G. Smith,[122] K. Stenson,[122] K. A. Ulmer,[122] S. R. Wagner,[122] S. L. Zang,[122] L. Agostino,[123] J. Alexander,[123] D. Cassel,[123] A. Chatterjee,[123] S. Das,[123] N. Eggert,[123] L. K. Gibbons,[123] B. Heltsley,[123] W. Hopkins,[123] A. Khukhunaishvili,[123] B. Kreis,[123] G. Nicolas Kaufman,[123] J. R. Patterson,[123] D. Puigh,[123] A. Ryd,[123] X. Shi,[123] W. Sun,[123] W. D. Teo,[123] J. Thom,[123] J. Thompson,[123] J. Vaughan,[123] Y. Weng,[123] L. Winstrom,[123] P. Wittich,[123] A. Biselli,[124] G. Cirino,[124] D. Winn,[124] S. Abdullin,[125] M. Albrow,[125] J. Anderson,[125] G. Apollinari,[125] M. Atac,[125] J. A. Bakken,[125] S. Banerjee,[125] L. A. T. Bauerdick,[125] A. Beretvas,[125] J. Berryhill,[125] P. C. Bhat,[125] I. Bloch,[125] F. Borcherding,[125] K. Burkett,[125] J. N. Butler,[125] V. Chetluru,[125] H. W. K. Cheung,[125] F. Chlebana,[125] S. Cihangir,[125] W. Cooper,[125] D. P. Eartly,[125] V. D. Elvira,[125] S. Esen,[125] I. Fisk,[125] J. Freeman,[125] Y. Gao,[125] E. Gottschalk,[125] D. Green,[125] K. Gunthoti,[125] O. Gutsche,[125] J. Hanlon,[125] R. M. Harris,[125] J. Hirschauer,[125] B. Hooberman,[125] H. Jensen,[125] M. Johnson,[125] U. Joshi,[125] R. Khatiwada,[125] B. Klima,[125] K. Kousouris,[125] S. Kunori,[125] S. Kwan,[125] C. Leonidopoulos,[125] P. Limon,[125] D. Lincoln,[125] R. Lipton,[125] J. Lykken,[125] K. Maeshima,[125] J. M. Marraffino,[125] D. Mason,[125] P. McBride,[125] T. Miao,[125] K. Mishra,[125] S. Mrenna,[125] Y. Musienko,[125,qq] C. Newman-Holmes,[125] V. O'Dell,[125] R. Pordes,[125] O. Prokofyev,[125] N. Saoulidou,[125] E. Sexton-Kennedy,[125] S. Sharma,[125] W. J. Spalding,[125] L. Spiegel,[125] P. Tan,[125] L. Taylor,[125] S. Tkaczyk,[125] L. Uplegger,[125] E. W. Vaandering,[125] R. Vidal,[125] J. Whitmore,[125] W. Wu,[125] F. Yang,[125] F. Yumiceva,[125] J. C. Yun,[125] D. Acosta,[126] P. Avery,[126] D. Bourilkov,[126] M. Chen,[126] G. P. Di Giovanni,[126] D. Dobur,[126] A. Drozdetskiy,[126] R. D. Field,[126] M. Fisher,[126] Y. Fu,[126] I. K. Furic,[126] J. Gartner,[126] S. Goldberg,[126] B. Kim,[126] J. Konigsberg,[126] A. Korytov,[126] A. Kropivnitskaya,[126] T. Kypreos,[126] K. Matchev,[126] G. Mitselmakher,[126] L. Muniz,[126] Y. Pakhotin,[126] C. Prescott,[126] R. Remington,[126] M. Schmitt,[126] B. Scurlock,[126] P. Sellers,[126] N. Skhirtladze,[126] D. Wang,[126] J. Yelton,[126] M. Zakaria,[126] C. Ceron,[127] V. Gaultney,[127] L. Kramer,[127] L. M. Lebolo,[127] S. Linn,[127] P. Markowitz,[127] G. Martinez,[127] J. L. Rodriguez,[127] T. Adams,[128] A. Askew,[128] D. Bandurin,[128] J. Bochenek,[128] J. Chen,[128] B. Diamond,[128] S. V. Gleyzer,[128] J. Haas,[128] V. Hagopian,[128] M. Jenkins,[128] K. F. Johnson,[128] H. Prosper,[128] L. Quertenmont,[128] S. Sekmen,[128] V. Veeraraghavan,[128] M. M. Baarmand,[129] B. Dorney,[129] S. Guragain,[129] M. Hohlmann,[129] H. Kalakhety,[129] R. Ralich,[129] I. Vodopiyanov,[129] M. R. Adams,[130] I. M. Anghel,[130] L. Apanasevich,[130] Y. Bai,[130] V. E. Bazterra,[130] R. R. Betts,[130] J. Callner,[130] R. Cavanaugh,[130] C. Dragoiu,[130] L. Gauthier,[130] C. E. Gerber,[130] D. J. Hofman,[130] S. Khalatyan,[130] G. J. Kunde,[130,rr] F. Lacroix,[130] M. Malek,[130] C. O'Brien,[130] C. Silvestre,[130] A. Smoron,[130] D. Strom,[130] N. Varelas,[130] U. Akgun,[131] E. A. Albayrak,[131] B. Bilki,[131] W. Clarida,[131] F. Duru,[131] C. K. Lae,[131] E. McCliment,[131] J.-P. Merlo,[131] H. Mermerkaya,[131] A. Mestvirishvili,[131] A. Moeller,[131] J. Nachtman,[131] C. R. Newsom,[131] E. Norbeck,[131] J. Olson,[131] Y. Onel,[131] F. Ozok,[131] S. Sen,[131] J. Wetzel,[131] T. Yetkin,[131] K. Yi,[131] B. A. Barnett,[132] B. Blumenfeld,[132] A. Bonato,[132] C. Eskew,[132] D. Fehling,[132] G. Giurgiu,[132] A. V. Gritsan,[132] G. Hu,[132] P. Maksimovic,[132] S. Rappoccio,[132] M. Swartz,[132] N. V. Tran,[132] A. Whitbeck,[132] P. Baringer,[133] A. Bean,[133] G. Benelli,[133] O. Grachov,[133] M. Murray,[133] D. Noonan,[133] S. Sanders,[133] J. S. Wood,[133] V. Zhukova,[133] A. F. Barfuss,[134] T. Bolton,[134] I. Chakaberia,[134] A. Ivanov,[134] M. Makouski,[134] Y. Maravin,[134] S. Shrestha,[134] I. Svintradze,[134] Z. Wan,[134] J. Gronberg,[135] D. Lange,[135] D. Wright,[135] A. Baden,[136] M. Boutemeur,[136] S. C. Eno,[136] D. Ferencek,[136] J. A. Gomez,[136] N. J. Hadley,[136] R. G. Kellogg,[136] M. Kirn,[136] Y. Lu,[136] A. C. Mignerey,[136] K. Rossato,[136] P. Rumerio,[136] F. Santanastasio,[136] A. Skuja,[136] J. Temple,[136] M. B. Tonjes,[136] S. C. Tonwar,[136] E. Twedt,[136] B. Alver,[137] G. Bauer,[137] J. Bendavid,[137] W. Busza,[137] E. Butz,[137] I. A. Cali,[137]

M. Chan,[137] V. Dutta,[137] P. Everaerts,[137] G. Gomez Ceballos,[137] M. Goncharov,[137] K. A. Hahn,[137] P. Harris,[137] Y. Kim,[137] M. Klute,[137] Y.-J. Lee,[137] W. Li,[137] C. Loizides,[137] P. D. Luckey,[137] T. Ma,[137] S. Nahn,[137] C. Paus,[137] D. Ralph,[137] C. Roland,[137] G. Roland,[137] M. Rudolph,[137] G. S. F. Stephans,[137] K. Sumorok,[137] K. Sung,[137] E. A. Wenger,[137] S. Xie,[137] M. Yang,[137] Y. Yilmaz,[137] A. S. Yoon,[137] M. Zanetti,[137] P. Cole,[138] S. I. Cooper,[138] P. Cushman,[138] B. Dahmes,[138] A. De Benedetti,[138] P. R. Dudero,[138] G. Franzoni,[138] J. Haupt,[138] K. Klapoetke,[138] Y. Kubota,[138] J. Mans,[138] V. Rekovic,[138] R. Rusack,[138] M. Sasseville,[138] A. Singovsky,[138] L. M. Cremaldi,[139] R. Godang,[139] R. Kroeger,[139] L. Perera,[139] R. Rahmat,[139] D. A. Sanders,[139] D. Summers,[139] K. Bloom,[140] S. Bose,[140] J. Butt,[140] D. R. Claes,[140] A. Dominguez,[140] M. Eads,[140] J. Keller,[140] T. Kelly,[140] I. Kravchenko,[140] J. Lazo-Flores,[140] H. Malbouisson,[140] S. Malik,[140] G. R. Snow,[140] U. Baur,[141] A. Godshalk,[141] I. Iashvili,[141] S. Jain,[141] A. Kharchilava,[141] A. Kumar,[141] S. P. Shipkowski,[141] K. Smith,[141] G. Alverson,[142] E. Barberis,[142] D. Baumgartel,[142] O. Boeriu,[142] M. Chasco,[142] S. Reucroft,[142] J. Swain,[142] D. Wood,[142] J. Zhang,[142] A. Anastassov,[143] A. Kubik,[143] N. Odell,[143] R. A. Ofierzynski,[143] B. Pollack,[143] A. Pozdnyakov,[143] M. Schmitt,[143] S. Stoynev,[143] M. Velasco,[143] S. Won,[143] L. Antonelli,[144] D. Berry,[144] M. Hildreth,[144] C. Jessop,[144] D. J. Karmgard,[144] J. Kolb,[144] T. Kolberg,[144] K. Lannon,[144] W. Luo,[144] S. Lynch,[144] N. Marinelli,[144] D. M. Morse,[144] T. Pearson,[144] R. Ruchti,[144] J. Slaunwhite,[144] N. Valls,[144] M. Wayne,[144] J. Ziegler,[144] B. Bylsma,[145] L. S. Durkin,[145] J. Gu,[145] C. Hill,[145] P. Killewald,[145] K. Kotov,[145] M. Rodenburg,[145] G. Williams,[145] N. Adam,[146] E. Berry,[146] P. Elmer,[146] D. Gerbaudo,[146] V. Halyo,[146] P. Hebda,[146] A. Hunt,[146] J. Jones,[146] E. Laird,[146] D. Lopes Pegna,[146] D. Marlow,[146] T. Medvedeva,[146] M. Mooney,[146] J. Olsen,[146] P. Piroué,[146] X. Quan,[146] H. Saka,[146] D. Stickland,[146] C. Tully,[146] J. S. Werner,[146] A. Zuranski,[146] J. G. Acosta,[147] X. T. Huang,[147] A. Lopez,[147] H. Mendez,[147] S. Oliveros,[147] J. E. Ramirez Vargas,[147] A. Zatserklyaniy,[147] E. Alagoz,[148] V. E. Barnes,[148] G. Bolla,[148] L. Borrello,[148] D. Bortoletto,[148] A. Everett,[148] A. F. Garfinkel,[148] L. Gutay,[148] Z. Hu,[148] M. Jones,[148] O. Koybasi,[148] M. Kress,[148] A. T. Laasanen,[148] N. Leonardo,[148] C. Liu,[148] V. Maroussov,[148] P. Merkel,[148] D. H. Miller,[148] N. Neumeister,[148] I. Shipsey,[148] D. Silvers,[148] A. Svyatkovskiy,[148] H. D. Yoo,[148] J. Zablocki,[148] Y. Zheng,[148] P. Jindal,[149] N. Parashar,[149] C. Boulahouache,[150] V. Cuplov,[150] K. M. Ecklund,[150] F. J. M. Geurts,[150] B. P. Padley,[150] R. Redjimi,[150] J. Roberts,[150] J. Zabel,[150] B. Betchart,[151] A. Bodek,[151] Y. S. Chung,[151] R. Covarelli,[151] P. de Barbaro,[151] R. Demina,[151] Y. Eshaq,[151] H. Flacher,[151] A. Garcia-Bellido,[151] P. Goldenzweig,[151] Y. Gotra,[151] J. Han,[151] A. Harel,[151] D. C. Miner,[151] D. Orbaker,[151] G. Petrillo,[151] D. Vishnevskiy,[151] M. Zielinski,[151] A. Bhatti,[152] R. Ciesielski,[152] L. Demortier,[152] K. Goulianos,[152] G. Lungu,[152] C. Mesropian,[152] M. Yan,[152] O. Atramentov,[153] A. Barker,[153] D. Duggan,[153] Y. Gershtein,[153] R. Gray,[153] E. Halkiadakis,[153] D. Hidas,[153] D. Hits,[153] A. Lath,[153] S. Panwalkar,[153] R. Patel,[153] A. Richards,[153] K. Rose,[153] S. Schnetzer,[153] S. Somalwar,[153] R. Stone,[153] S. Thomas,[153] G. Cerizza,[154] M. Hollingsworth,[154] S. Spanier,[154] Z. C. Yang,[154] A. York,[154] J. Asaadi,[155] R. Eusebi,[155] J. Gilmore,[155] A. Gurrola,[155] T. Kamon,[155] V. Khotilovich,[155] R. Montalvo,[155] C. N. Nguyen,[155] I. Osipenkov,[155] J. Pivarski,[155] A. Safonov,[155] S. Sengupta,[155] A. Tatarinov,[155] D. Toback,[155] M. Weinberger,[155] N. Akchurin,[156] J. Damgov,[156] C. Jeong,[156] K. Kovitanggoon,[156] S. W. Lee,[156] Y. Roh,[156] A. Sill,[156] I. Volobouev,[156] R. Wigmans,[156] E. Yazgan,[156] E. Appelt,[157] E. Brownson,[157] D. Engh,[157] C. Florez,[157] W. Gabella,[157] M. Issah,[157] W. Johns,[157] P. Kurt,[157] C. Maguire,[157] A. Melo,[157] P. Sheldon,[157] S. Tuo,[157] J. Velkovska,[157] M. W. Arenton,[158] M. Balazs,[158] S. Boutle,[158] M. Buehler,[158] S. Conetti,[158] B. Cox,[158] B. Francis,[158] R. Hirosky,[158] A. Ledovskoy,[158] C. Lin,[158] C. Neu,[158] R. Yohay,[158] S. Gollapinni,[159] R. Harr,[159] P. E. Karchin,[159] P. Lamichhane,[159] M. Mattson,[159] C. Milstène,[159] A. Sakharov,[159] M. Anderson,[160] M. Bachtis,[160] J. N. Bellinger,[160] D. Carlsmith,[160] S. Dasu,[160] J. Efron,[160] K. Flood,[160] L. Gray,[160] K. S. Grogg,[160] M. Grothe,[160] R. Hall-Wilton,[160,a] M. Herndon,[160] P. Klabbers,[160] J. Klukas,[160] A. Lanaro,[160] C. Lazaridis,[160] J. Leonard,[160] R. Loveless,[160] A. Mohapatra,[160] D. Reeder,[160] I. Ross,[160] A. Savin,[160] W. H. Smith,[160] J. Swanson,[160] and M. Weinberg[160]

(CMS Collaboration)

[1]*Yerevan Physics Institute, Yerevan, Armenia*
[2]*Institut für Hochenergiephysik der OeAW, Wien, Austria*
[3]*National Centre for Particle and High Energy Physics, Minsk, Belarus*
[4]*Universiteit Antwerpen, Antwerpen, Belgium*
[5]*Vrije Universiteit Brussel, Brussel, Belgium*
[6]*Université Libre de Bruxelles, Bruxelles, Belgium*
[7]*Ghent University, Ghent, Belgium*
[8]*Université Catholique de Louvain, Louvain-la Neuve, Belgium*
[9]*Université de Mons, Mons, Belgium*
[10]*Centro Brasileiro de Pesquisas Fisicas, Rio de Janeiro, Brazil*
[11]*Universidade do Estado do Rio de Janeiro, Rio de Janeiro, Brazil*
[12]*Instituto de Fisica Teorica, Universidade Estadual Paulista, Sao Paulo, Brazil*
[13]*Institute for Nuclear Research and Nuclear Energy, Sofia, Bulgaria*
[14]*University of Sofia, Sofia, Bulgaria*
[15]*Institute of High Energy Physics, Beijing, China*
[16]*State Key Laboratory of Nuclear Physics and Technology, Peking University, Beijing, China*
[17]*Universidad de Los Andes, Bogota, Colombia*

[18]*Technical University of Split, Split, Croatia*
[19]*University of Split, Split, Croatia*
[20]*Institute Rudjer Boskovic, Zagreb, Croatia*
[21]*University of Cyprus, Nicosia, Cyprus*
[22]*Charles University, Prague, Czech Republic*
[23]*Academy of Scientific Research and Technology of the Arab Republic of Egypt, Egyptian Network of High Energy Physics, Cairo, Egypt*
[24]*National Institute of Chemical Physics and Biophysics, Tallinn, Estonia*
[25]*Department of Physics, University of Helsinki, Helsinki, Finland*
[26]*Helsinki Institute of Physics, Helsinki, Finland*
[27]*Lappeenranta University of Technology, Lappeenranta, Finland*
[28]*Laboratoire d'Annecy-le-Vieux de Physique des Particules, IN2P3-CNRS, Annecy-le-Vieux, France*
[29]*Direction des Sciences de la Matière/Institut de Recherche sur les lois Fondamentales de l'Univers (DSM/IRFU),*
CEA/Saclay, Gif-sur-Yvette, France
[30]*Laboratoire Leprince-Ringuet, Ecole Polytechnique, IN2P3-CNRS, Palaiseau, France*
[31]*Institut Pluridisciplinaire Hubert Curien, Université de Strasbourg, Université de Haute Alsace Mulhouse, CNRS/IN2P3, Strasbourg, France*
[32]*Centre de Calcul de l'Institut National de Physique Nucleaire et de Physique des Particules (IN2P3), Villeurbanne, France*
[33]*Université de Lyon, Université Claude Bernard Lyon 1, CNRS-IN2P3, Institut de Physique Nucléaire de Lyon, Villeurbanne, France*
[34]*E. Andronikashvili Institute of Physics, Academy of Science, Tbilisi, Georgia*
[35]*Institute of High Energy Physics and Informatization, Tbilisi State University, Tbilisi, Georgia*
[36]*RWTH Aachen University, I. Physikalisches Institut, Aachen, Germany*
[37]*RWTH Aachen University, III. Physikalisches Institut A, Aachen, Germany*
[38]*RWTH Aachen University, III. Physikalisches Institut B, Aachen, Germany*
[39]*Deutsches Elektronen-Synchrotron, Hamburg, Germany*
[40]*University of Hamburg, Hamburg, Germany*
[41]*Institut für Experimentelle Kernphysik, Karlsruhe, Germany*
[42]*Institute of Nuclear Physics "Demokritos," Aghia Paraskevi, Greece*
[43]*University of Athens, Athens, Greece*
[44]*University of Ioánnina, Ioánnina, Greece*
[45]*KFKI Research Institute for Particle and Nuclear Physics, Budapest, Hungary*
[46]*Institute of Nuclear Research ATOMKI, Debrecen, Hungary*
[47]*University of Debrecen, Debrecen, Hungary*
[48]*Panjab University, Chandigarh, India*
[49]*University of Delhi, Delhi, India*
[50]*Bhabha Atomic Research Centre, Mumbai, India*
[51]*Tata Institute of Fundamental Research–EHEP, Mumbai, India*
[52]*Tata Institute of Fundamental Research–HECR, Mumbai, India*
[53]*Institute for Research and Fundamental Sciences (IPM), Tehran, Iran*
[54a]*INFN Sezione di Bari, Bari, Italy*
[54b]*Università di Bari, Bari, Italy*
[54c]*Politecnico di Bari, Bari, Italy*
[55a]*INFN Sezione di Bologna, Bologna, Italy*
[55b]*Università di Bologna, Bologna, Italy*
[56a]*INFN Sezione di Catania, Catania, Italy*
[56b]*Università di Catania, Catania, Italy*
[57a]*INFN Sezione di Firenze, Firenze, Italy*
[57b]*Università di Firenze, Firenze, Italy*
[58]*INFN Laboratori Nazionali di Frascati, Frascati, Italy*
[59]*INFN Sezione di Genova, Genova, Italy*
[60a]*INFN Sezione di Milano-Biccoca, Milano, Italy*
[60b]*Università di Milano-Bicocca, Milano, Italy*
[61a]*INFN Sezione di Napoli, Napoli, Italy*
[61b]*Università di Napoli "Federico II", Napoli, Italy*
[62a]*INFN Sezione di Padova, Padova, Italy*
[62b]*Università di Padova, Padova, Italy*
[62c]*Università di Trento (Trento), Padova, Italy*
[63a]*INFN Sezione di Pavia, Pavia, Italy*
[63b]*Università di Pavia, Pavia, Italy*
[64a]*INFN Sezione di Perugia, Perugia, Italy*

[64b] *Università di Perugia, Perugia, Italy*
[65a] *INFN Sezione di Pisa, Pisa, Italy*
[65b] *Università di Pisa, Pisa, Italy*
[65c] *Scuola Normale Superiore di Pisa, Pisa, Italy*
[66a] *INFN Sezione di Roma, Roma, Italy*
[66b] *Università di Roma "La Sapienza," Roma, Italy*
[67a] *INFN Sezione di Torino, Torino, Italy*
[67b] *Università di Torino, Torino, Italy*
[67c] *Università del Piemonte Orientale (Novara), Torino, Italy*
[68a] *INFN Sezione di Trieste, Trieste, Italy*
[68b] *Università di Trieste, Trieste, Italy*
[69] *Kangwon National University, Chunchon, Korea*
[70] *Kyungpook National University, Daegu, Korea*
[71] *Chonnam National University, Institute for Universe and Elementary Particles, Kwangju, Korea*
[72] *Korea University, Seoul, Korea*
[73] *University of Seoul, Seoul, Korea*
[74] *Sungkyunkwan University, Suwon, Korea*
[75] *Vilnius University, Vilnius, Lithuania*
[76] *Centro de Investigacion y de Estudios Avanzados del IPN, Mexico City, Mexico*
[77] *Universidad Iberoamericana, Mexico City, Mexico*
[78] *Benemerita Universidad Autonoma de Puebla, Puebla, Mexico*
[79] *Universidad Autónoma de San Luis Potosí, San Luis Potosí, Mexico*
[80] *University of Auckland, Auckland, New Zealand*
[81] *University of Canterbury, Christchurch, New Zealand*
[82] *National Centre for Physics, Quaid-I-Azam University, Islamabad, Pakistan*
[83] *Institute of Experimental Physics, Faculty of Physics, University of Warsaw, Warsaw, Poland*
[84] *Soltan Institute for Nuclear Studies, Warsaw, Poland*
[85] *Laboratório de Instrumentação e Física Experimental de Partículas, Lisboa, Portugal*
[86] *Joint Institute for Nuclear Research, Dubna, Russia*
[87] *Petersburg Nuclear Physics Institute, Gatchina (St. Petersburg), Russia*
[88] *Institute for Nuclear Research, Moscow, Russia*
[89] *Institute for Theoretical and Experimental Physics, Moscow, Russia*
[90] *Moscow State University, Moscow, Russia*
[91] *P. N. Lebedev Physical Institute, Moscow, Russia*
[92] *State Research Center of Russian Federation, Institute for High Energy Physics, Protvino, Russia*
[93] *University of Belgrade, Faculty of Physics and Vinca Institute of Nuclear Sciences, Belgrade, Serbia*
[94] *Centro de Investigaciones Energéticas Medioambientales y Tecnológicas (CIEMAT), Madrid, Spain*
[95] *Universidad Autónoma de Madrid, Madrid, Spain*
[96] *Universidad de Oviedo, Oviedo, Spain*
[97] *Instituto de Física de Cantabria (IFCA), CSIC-Universidad de Cantabria, Santander, Spain*
[98] *CERN, European Organization for Nuclear Research, Geneva, Switzerland*
[99] *Paul Scherrer Institut, Villigen, Switzerland*
[100] *Institute for Particle Physics, ETH Zurich, Zurich, Switzerland*
[101] *Universität Zürich, Zurich, Switzerland*
[102] *National Central University, Chung-Li, Taiwan*
[103] *National Taiwan University (NTU), Taipei, Taiwan*
[104] *Cukurova University, Adana, Turkey*
[105] *Middle East Technical University, Physics Department, Ankara, Turkey*
[106] *Bogazici University, Istanbul, Turkey*
[107] *National Scientific Center, Kharkov Institute of Physics and Technology, Kharkov, Ukraine*
[108] *University of Bristol, Bristol, United Kingdom*
[109] *Rutherford Appleton Laboratory, Didcot, United Kingdom*
[110] *Imperial College, London, United Kingdom*
[111] *Brunel University, Uxbridge, United Kingdom*
[112] *Baylor University, Waco, Texas 76798, USA*
[113] *Boston University, Boston, Massachusetts 02215, USA*
[114] *Brown University, Providence, Rhode Island 02906, USA*
[115] *University of California, Davis, Davis, California 95616, USA*

[116] *University of California, Los Angeles, Los Angeles, California 90095, USA*
[117] *University of California, Riverside, Riverside, California 92507, USA*
[118] *University of California, San Diego, La Jolla, California 92037, USA*
[119] *University of California, Santa Barbara, Santa Barbara, California 93106, USA*
[120] *California Institute of Technology, Pasadena, California 91125, USA*
[121] *Carnegie Mellon University, Pittsburgh, Pennsylvania 15213, USA*
[122] *University of Colorado at Boulder, Boulder, Colorado 80309, USA*
[123] *Cornell University, Ithaca, New York 14850, USA*
[124] *Fairfield University, Fairfield, Connecticut 06824, USA*
[125] *Fermi National Accelerator Laboratory, Batavia, Illinois 60510, USA*
[126] *University of Florida, Gainesville, Florida 32611, USA*
[127] *Florida International University, Miami, Florida 33199, USA*
[128] *Florida State University, Tallahassee, Florida 32306, USA*
[129] *Florida Institute of Technology, Melbourne, Florida 32901, USA*
[130] *University of Illinois at Chicago (UIC), Chicago, Illinois 60607, USA*
[131] *The University of Iowa, Iowa City, Iowa 52242, USA*
[132] *Johns Hopkins University, Baltimore, Maryland 21218, USA*
[133] *The University of Kansas, Lawrence, Kansas 66045, USA*
[134] *Kansas State University, Manhattan, Kansas 66506, USA*
[135] *Lawrence Livermore National Laboratory, Livermore, California 94550, USA*
[136] *University of Maryland, College Park, Maryland 20742, USA*
[137] *Massachusetts Institute of Technology, Cambridge, Massachusetts 02139, USA*
[138] *University of Minnesota, Minneapolis, Minnesota 55455, USA*
[139] *University of Mississippi, University, Mississippi 38677, USA*
[140] *University of Nebraska-Lincoln, Lincoln, Nebraska 68588, USA*
[141] *State University of New York at Buffalo, Buffalo, New York 14260, USA*
[142] *Northeastern University, Boston, Massachusetts 02115, USA*
[143] *Northwestern University, Evanston, Illinois 60208, USA*
[144] *University of Notre Dame, Notre Dame, Indiana 46556, USA*
[145] *The Ohio State University, Columbus, Ohio 43210, USA*
[146] *Princeton University, Princeton, New Jersey 08544, USA*
[147] *University of Puerto Rico, Mayaguez, Puerto Rico*
[148] *Purdue University, West Lafayette, Indiana 47907, USA*
[149] *Purdue University Calumet, Hammond, Indiana 46323, USA*
[150] *Rice University, Houston, Texas 77251, USA*
[151] *University of Rochester, Rochester, New York 14642, USA*
[152] *The Rockefeller University, New York, New York 10065, USA*
[153] *Rutgers, The State University of New Jersey, Piscataway, New Jersey 08854, USA*
[154] *University of Tennessee, Knoxville, Tennessee 37916, USA*
[155] *Texas A&M University, College Station, Texas 77843, USA*
[156] *Texas Tech University, Lubbock, Texas 79409, USA*
[157] *Vanderbilt University, Nashville, Tennessee 37240, USA*
[158] *University of Virginia, Charlottesville, Virginia 22904, USA*
[159] *Wayne State University, Detroit, Michigan 48202, USA*
[160] *University of Wisconsin, Madison, Wisconsin 53706, USA*

[a] Also at CERN, European Organization for Nuclear Research, Geneva, Switzerland.
[b] Also at Universidade Federal do ABC, Santo Andre, Brazil.
[c] Also at Laboratoire Leprince-Ringuet, Ecole Polytechnique, IN2P3-CNRS, Palaiseau, France.
[d] Also at Suez Canal University, Suez, Egypt.
[e] Also at British University, Cairo, Egypt.
[f] Also at Fayoum University, El-Fayoum, Egypt.
[g] Also at Soltan Institute for Nuclear Studies, Warsaw, Poland.
[h] Also at Massachusetts Institute of Technology, Cambridge, MA 02139.
[i] Also at Université de Haute-Alsace, Mulhouse, France.
[j] Also at Deceased.
[k] Also at Brandenburg University of Technology, Cottbus, Germany.
[l] Also at Moscow State University, Moscow, Russia.
[m] Also at Institute of Nuclear Research ATOMKI, Debrecen, Hungary.

[n]Also at Eötvös Loránd University, Budapest, Hungary.

[o]Also at Tata Institute of Fundamental Research–HECR, Mumbai, India.

[p]Also at University of Visva-Bharati, Santiniketan, India.

[q]Also at Facoltà Ingegneria Università di Roma "La Sapienza," Roma, Italy.

[r]Also at Università della Basilicata, Potenza, Italy.

[s]Also at Laboratori Nazionali di Legnaro dell' INFN, Legnaro, Italy.

[t]Also at Università degli studi di Siena, Siena, Italy.

[u]Also at Faculty of Physics of University of Belgrade, Belgrade, Serbia.

[v]Also at University of California, Los Angeles, Los Angeles, CA 90095.

[w]Also at University of Florida, Gainesville, FL 32611.

[x]Also at Université de Genève, Geneva, Switzerland.

[y]Also at Scuola Normale e Sezione dell' INFN, Pisa, Italy.

[z]Also at (a) INFN Sezione di Roma; (b) Università di Roma "La Sapienza," Roma, Italy.

[aa]Also at University of Athens, Athens, Greece.

[bb]Also at California Institute of Technology, Pasadena, CA 91125.

[cc]Also at The University of Kansas, Lawrence, KS 66045.

[dd]Also at Institute for Theoretical and Experimental Physics, Moscow, Russia.

[ee]Also at Paul Scherrer Institut, Villigen, Switzerland.

[ff]Also at University of Belgrade, Faculty of Physics and Vinca Institute of Nuclear Sciences, Belgrade, Serbia.

[gg]Also at Mersin University, Mersin, Turkey.

[hh]Also at Adiyaman University, Adiyaman, Turkey.

[ii]Also at Izmir Institute of Technology, Izmir, Turkey.

[jj]Also at Kafkas University, Kars, Turkey.

[kk]Also at Suleyman Demirel University, Isparta, Turkey.

[ll]Also at Ege University, Izmir, Turkey.

[mm]Also at Rutherford Appleton Laboratory, Didcot, United Kingdom.

[nn]Also at School of Physics and Astronomy, University of Southampton, Southampton, United Kingdom.

[oo]Also at (a) INFN Sezione di Perugia; (b) Università di Perugia, Perugia, Italy.

[pp]Also at Utah Valley University, Orem, UT 84058 .

[qq]Also at Institute for Nuclear Research, Moscow, Russia.

[rr]Also at Los Alamos National Laboratory, Los Alamos, NM 87545.